

# Stochastic Dynamics of the Multi-State Voter Model over a Network based on Interacting Cliques and Zealot Candidates

Filippo Palombi<sup>a\*</sup> and Simona Toti<sup>b</sup>

<sup>a</sup>ENEA – Italian Agency for New Technologies, Energy and Sustainable Economic Development, *Via Enrico Fermi 45, 00040 Frascati – Italy*

<sup>b</sup>ISTAT – Istituto Nazionale di Statistica, *Via Cesare Balbo 16, 00184 Rome – Italy*

April 2014

## Abstract

The stochastic dynamics of the multi-state voter model is investigated on a class of complex networks made of non-overlapping cliques, each hosting a political candidate and interacting with the others via Erdős-Rényi links. Numerical simulations of the model are interpreted in terms of an *ad-hoc* mean field theory, specifically tuned to resolve the inter/intra-clique interactions. Under a proper definition of the thermodynamic limit (with the average degree of the agents kept fixed while increasing the network size), the model is found to display the empirical scaling discovered by Fortunato and Castellano (2007) [1], while the vote distribution resembles roughly that observed in Brazilian elections.

## 1 Introduction

In a fairly recent paper [1], Fortunato and Castellano (FC) show that the excess of the number of votes received in proportional elections by candidates over the average number of votes per intra-party competitor has a universal distribution, invariant in time and independent of the country. The analysis performed in [1] focuses in particular on the political elections held along the past fifty years in Italy, Poland and Finland. In order to interpret the empirical evidence, FC propose a *word of mouth* model, where political opinions originate from the candidates and propagate down stochastic trees. With an appropriate choice of the underlying parameters, the model reproduces faithfully the observed voting behavior.

A more recent extension of the above analysis to a larger pool of countries [2] confirms the universal trend in Denmark and Estonia, but proves it to be hopelessly broken in countries such as Brazil, Slovenia, Greece, *etc.* In each of these, the probability law of the intra-party excess of votes displays specific deviations from the universal FC curve, while persisting in time. Therefore, the discrepancies — as the authors of [2] claim — are “*likely to be due to peculiar differences in the election rules*”. An interesting and not understood case is indeed represented by Brazil, which has been first studied in [3]. Here, voting

---

\*Corresponding author. E-mail: [filippo.palombi@enea.it](mailto:filippo.palombi@enea.it)

is compulsory, though a justification form for not voting can be filled at election centers and post offices. Compulsory voting can be hardly encoded in the word of mouth model by FC without introducing major modifications, thus it makes sense to approach the Brazilian case differently. The search for a dynamical model reproducing at least qualitatively the Brazilian pattern is the main phenomenological motivation for the present paper.

Notoriously, a model where voting is compulsory is the voter model (VM) [4, 5], in that here every agent expresses a preference at each time step of the stochastic dynamics. In addition, political positions in the VM differ only by their tag, just like candidates in the word of mouth model. The reason why a simple toy model such as the VM could effectively reproduce the universalities of real elections and their breaking patterns lies in the guiding principle of complexity theory that a *complex* behavior often emerges from *simple* rules. Of course, the model needs to be properly adapted to catch the main features of the intra-party dynamics in proportional elections with compulsory voting, yet much is already present in the literature:

- First of all, the VM is a binary model, unfit to describe elections with more than two candidates. This difficulty is easily overcome by turning to the multi-state variant considered with different purposes in [6, 7, 8, 9].
- Secondly, the stochastic dynamics of both the binary VM and its multi-state variant drives ultimately the system towards consensus, a uniform state where all agents share the same political preference. A quantitative description of consensus formation in the multi-state VM has been recently given in [10] in terms of mean field theory (MFT). Needless to say, consensus states have been nowhere near observed in political elections, thus they should not be contemplated by any serious attempt to describe empirical data in a semi-realistic fashion. The simplest way to avoid them seems to be the use of stubborn agents (also known as *zealots*), that is to say agents who never change political preference, while taking part in the stochastic dynamics as opinion donors. Zealots have been originally introduced in [11] in the framework of the binary VM and have been subsequently used to investigate several aspects of opinion dynamics (see for instance [12, 13, 14, 15, 16, 17]). They have also been used in the context of the multi-state VM, see for instance [18] for an analysis of the three-party constrained VM in presence of committed agents. In principle zealots can model both political activists and candidates. In the present paper, we use them as list candidates.
- Thirdly, if candidates exert their influence on the neighbor voters by letting them change opinion according to the passive interaction rule defining the VM, their effect at macroscopic level depends certainly on the topological structure of the social network they are part of and the long-range competition they engage with other candidates. This is to a large extent unexplored to-date. We consider a voter network partitioned into non-overlapping cliques (sub-networks where the agents are all pairwise connected), all having the same size. Each clique hosts one candidate and candidates belong all to the same party. Voters belonging to different cliques are then stochastically connected via Erdős-Rényi links. This kind of network resembles somewhat the small-worlds model by Watts-Strogatz [19], the differences being that *i*) cliques in the latter are overlapping before rewiring, *ii*) in our model there is no *re-wiring* at all, *iii*) the Watts-Strogatz model converges to an Erdős-Rényi network as the rewiring probability increases, whereas our network model converges to an almost complete graph upon increasing the frequency of the inter-clique links. In a sense, cliques play in our proposal a rôle analogous to the stochastic trees in the word of mouth model by FC. Yet, voters belonging to different trees never interact directly, whereas inter-clique interactions are essential to the opinion dynamics of our model.

We study the distribution of the excess of votes at equilibrium by means of Monte Carlo simulations and, in a range of values of the model parameters, we observe distributions resembling roughly that of

Brazilian elections. An analytic description of the numerical results is at least partly possible thanks to MFT, but in order to take into consideration the specific topology of the network, MFT has to be formulated in terms of clique variables. Using the standard machinery of the Master Equation [20], we perform a Kramers–Moyal expansion and derive the corresponding Fokker–Planck (FP) equation. The drift equations obtained by suppressing the diffusion term in the latter can be analytically solved. Average values are thus calculated exactly and show a perfect agreement with those obtained numerically. In order to solve the complete FP equation, we simulate the stochastic process associated to it and discuss the effect of time discretization by considering two different recipes to enforce boundary reflections.

Here is a plan of the paper. In sect. 2, we define precisely the network, the stochastic dynamics and the thermodynamic limit of the model. In sect. 3, we report on some Monte Carlo simulations of the autocorrelation time, the average values of the clique variables and the distribution of the intra-party excess of votes. In sect. 4, we derive the FP equation and calculate the average values in MFT. Sect. 5 is devoted to a discussion of the stochastic process associated to the FP equation. Conclusions are drawn in sect. 6. In appendix A, we discuss some theoretical aspects of an expansion of the probability density of MFT based on Dirichlet distributions. Specifically, we examine the analytic structure of the contributions to the distribution of the excess of votes arising from it.

## 2 Definition of the model

### 2.1 Voter network

We consider a social network described by an undirected graph  $\mathcal{G} = (V, E)$ . An element  $x \in V$  represents a voter, while an edge  $(x, y) \in E$  indicates the acquaintance  $x, y \in V$  share. Each voter expresses a political preference as an element of  $\mathcal{W} = \{1, 2, \dots, Q\}$ , with  $Q \geq 2$ . We denote by  $X = \mathcal{W}^V$  the space of voter configurations: if  $\eta(\cdot) \in X$  and  $x \in V$ , then  $\eta(x)$  represents the political preference of  $x$  in  $\eta(\cdot)$ . We assume that  $Z = \{z_1, \dots, z_Q\} \subset V$  is a special subset of voters. Elements of  $Z$  are identified with list candidates and fulfill  $\eta(z_i) = i$  at all times, *i.e.* the state space is actually a proper subset  $\bar{X} \subset X$ . We denote by  $V_0 = V \setminus Z$  the set of the *dynamic* voters. We also assume that  $\mathcal{G}$  decomposes into  $Q$  cliques of equal size, each hosting a candidate. More precisely, we first introduce a partition  $\{C_i\}_{i=1}^Q$ , with  $C_i \subset V$  and

$$\bullet \quad V = \bigcup_{i=1}^Q C_i; \tag{2.1}$$

$$\bullet \quad C_i \cap C_j = \emptyset \quad \text{and} \quad |C_i| = |C_j| \quad \text{if} \quad i \neq j; \tag{2.2}$$

$$\bullet \quad z_i \in C_i, \quad i = 1, \dots, Q. \tag{2.3}$$

Then, we group edges according to the position of their end-points in  $\{C_i\}$  by defining the sets

$$E_{ij} = \{(x, y) \in E : x \in C_i \text{ and } y \in C_j\}. \tag{2.4}$$

We finally request  $(x, y) \in E_{ii}, \forall x, y \in C_i$ . In addition, we assume that candidates are disconnected from cliques different than their own: given  $1 \leq i, j \leq Q$  and  $i \neq j$ ,  $(z_i, y) \notin E_{i,j}, \forall y \in C_j$ . Connections between different cliques are random and modeled according to an Erdős–Rényi model with link probability  $p \in (0, 1]$ , namely

$$\text{given } i \neq j, x \in C_i/\{z_i\} \text{ and } y \in C_j/\{z_j\}, \text{ then } \text{prob}\{(x, y) \in E_{ij}\} = p. \tag{2.5}$$

We now introduce some definitions, which set-up the language of the clique MFT and are used in the sequel. Given  $\eta(\cdot) \in \bar{X}$ , we define

$$\eta_k = \{x \in V : \eta(x) = k\}, \quad k = 1, \dots, Q. \tag{2.6}$$

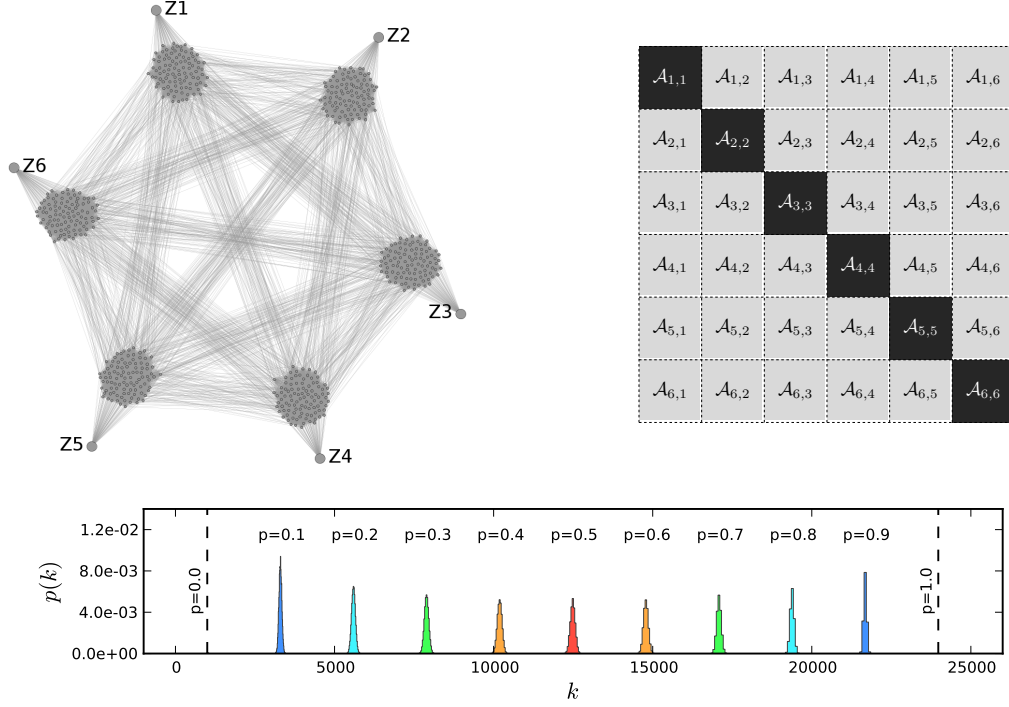


**Figure 1** – *Top left*: an illustrative network sample with  $|V| = 600$ ,  $Q = 6$  and  $p = 0.01$ . Candidates are highlighted. *Top right*: average structure of the adjacency matrix  $\mathcal{A}$  of the network at  $Q = 6$  and ordering function  $s$  as in eqs. (2.11)–(2.12); black (gray) squares describe dense intra-clique (sparse inter-clique) links. *Bottom*: distributions of the agent degree  $k$  for a network with  $|V| = 24,000$  and  $Q = 24$ .

Accordingly,  $v_k = |\eta_k|$  represents the number of votes for the candidate  $z_k$  in  $\eta(\cdot)$ . Analogously, we define

$$\eta_k^{(i)} = \{x \in C_i : \eta(x) = k\}, \quad i, k = 1, \dots, Q. \quad (2.7)$$

Again,  $\eta_k^{(i)}$  represents the subset of voters for the candidate  $z_k$  belonging to  $C_i$  and we denote by  $v_k^{(i)} = |\eta_k^{(i)}|$  the number of votes for  $z_k$  within  $C_i$ . From our definitions, it follows trivially that  $\eta_k = \cup_{i=1}^Q \eta_k^{(i)}$  and  $V = \cup_{k=1}^Q \eta_k$ . Note that  $1 \leq v_k^{(k)} \leq |V|/Q$  since  $z_k \in C_k$ , whereas  $0 \leq v_k^{(i)} \leq |V|/Q - 1$  for  $k \neq i$  owing to the presence to the opposing zealot  $z_i$ . By consistency, we have

$$v_k = \sum_{i=1}^Q v_k^{(i)}. \quad (2.8)$$

Along the same lines, we define

$$\eta_{km} = \{(x, y) \in E : \eta(x) = k \text{ and } \eta(y) = m\}, \quad k, m = 1, \dots, Q. \quad (2.9)$$

For  $k \neq m$ ,  $\eta_{km}$  represents the subset of edges for which a voter for  $z_k$  may turn into a voter for  $z_m$  in  $\eta(\cdot)$  and the other way round. Analogously, we define

$$\eta_{km}^{(ij)} = \{(x, y) \in E_{ij} : \eta(x) = k \text{ and } \eta(y) = m\}, \quad i, j, k, m = 1, \dots, Q, \quad (2.10)$$

and for  $k \neq m$ , we interpret  $\eta_{km}^{(ij)}$  as before, except that now the transition may only occur owing to an interaction between a voter in  $C_i$  and one in  $C_j$ . Obviously, we have  $\eta_{km} = \cup_{i,j=1}^Q \eta_{km}^{(ij)}$ .

In Fig. 1 (top left) we show a network sample with  $|V| = 600$ ,  $Q = 6$  and  $p = 0.01^1$ , where candidates are highlighted. In the same figure (top right), we show the average structure of the adjacency matrix

<sup>1</sup>the graph has been produced by using Gephi with a Force Atlas layout, see ref. [21]

$\mathcal{A}$  of the network model at  $Q = 6$ , corresponding to sorting the elements of  $V$  according to an ordering function  $s : V \rightarrow \{0, 1, \dots, |V| - 1\}$ , such that

$$\bullet (k-1)\frac{|V|}{Q} \leq s(x) < k\frac{|V|}{Q}, \quad \text{if } x \in C_k, \quad k = 1, \dots, Q; \quad (2.11)$$

$$\bullet s(z_k) = (k-1)\frac{|V|}{Q}, \quad k = 1, \dots, Q. \quad (2.12)$$

Diagonal blocks  $\mathcal{A}_{kk}$  represent intra-clique acquaintances, probabilistic Erdős–Rényi links populate the off-diagonal blocks  $\mathcal{A}_{ik}$  and thick-white borders indicate the absence of extra-clique zealot-voter and extra-clique zealot-zealot links. Again in Fig. 1 (bottom), we show some distributions of the voter degree for a network with  $|V| = 24,000$  and  $Q = 24$ .

As mentioned in the introduction, this network model looks somewhat similar to the construction by Watts–Strogatz, provided we interpret  $p$  as the analogous of the rewiring probability, yet the reader will notice some relevant differences:

- i)* both our network and the Watts–Strogatz one have a regular structure at  $p = 0$ , with the agents grouped into cliques. Nevertheless, in the Watts–Strogatz model cliques overlap partially, whereas in ours they are fully disconnected;
- ii)* as  $p$  increases, the Watts–Strogatz model becomes progressively disordered and it eventually degenerates to a random graph at  $p = 1$ . By contrast, the level of disorder of our network increases only up to  $p = 1/2$ . At larger values of  $p$  the network becomes progressively reordered, until it turns into an almost complete graph at  $p = 1$  (recall that  $Z$  does not take part in the random wiring process);
- iii)* the average degree of our network is monotonic increasing in  $p$ .

## 2.2 Microscopic dynamics

A multi-state voter dynamics is assumed to run on top of  $\mathcal{G}$ . A voter  $x \in V_0$  waits an exponential random time with rate  $\gamma = 1$ , at which she flips to the vote of one of her neighbors, chosen with flat probability. The microscopic state at time  $t$  is an element  $\eta(\cdot, t) \in \bar{X}$ . As already stated in the previous section, zealots keep their vote constant, *i.e.*  $\eta(z_i, t) = i$  for  $i = 1, \dots, Q$  and  $t \in [0, \infty)$ . All other observables change in time. The microscopic dynamics is rigorously defined in terms of the Markov generator of the process,

$$\Omega f(\eta) = \sum_{x \in V_0} \sum_{k \in \mathcal{W}} c_\eta(x, k) \{f(\eta_{x,k}) - f(\eta)\}, \quad (2.13)$$

an operator acting on the set  $C(\bar{X})$  of the cylinder functions on  $\bar{X}$ . Here, we denote by

$$\eta_{x,k}(\cdot) = \begin{cases} \eta(z) & \text{if } z \neq x, \\ k & \text{if } z = x. \end{cases} \quad (2.14)$$

the microscopic state following a transition of voter  $x$  in favor of candidate  $z_k$ , while

$$c_\eta(x, k) = \mathbb{I}\{\eta(x) \neq k\} \frac{1}{|\text{adj}_V(x)|} \sum_{y \in \text{adj}_V(x)} \mathbb{I}\{\eta(y) = k\}, \quad (2.15)$$

represents the corresponding transition rate. Note that the sum over  $x$  defining the Markov generator extends to  $V_0$ , while the adjacency vector  $\text{adj}_V(x)$  includes all neighbors of  $x$  in  $V$ , to reflect the active

rôle of the candidates as opinion donors. In the sequel, we focus on the stochastic trajectory of the vector  $v = \{v_k^{(i)}\}_{i,k=1}^Q$ , which evolves in a subset of  $\{0, 1, \dots, |V|/Q\}^{Q \times Q}$  subject to the constraints

$$\begin{cases} \sum_{k=1}^Q v_k^{(i)}(t) = |V|/Q, \\ v_i^{(i)}(t) \geq 1, \end{cases} \quad i = 1, \dots, Q \quad \text{and} \quad t \in [0, \infty). \quad (2.16)$$

### 2.3 Thermodynamic limit

We wish to investigate the statistical properties of the model in the thermodynamic limit  $|V| \rightarrow \infty$ . In order to ensure that this limit is taken along a trajectory of constant physics, the geometric set-up has to be rescaled as  $|V|$  increases. To this aim, we look at the average degree of the voters,  $\mathbb{E}|\text{adj}_V(x)|$  with  $x \in V_0$ , where the expectation is taken over the network ensemble described in sect. 2.1. It holds

$$\mathbb{E}|\text{adj}_V(x)| = \delta_{\text{in}} + \delta_{\text{out}}, \quad (2.17)$$

where

$$\delta_{\text{in}} = \left( \frac{|V|}{Q} - 1 \right), \quad \delta_{\text{out}} = p(Q-1) \left( \frac{|V|}{Q} - 1 \right), \quad (2.18)$$

represent the intra- and extra-clique average degree. We keep both  $\delta_{\text{in}}$  and  $\delta_{\text{out}}$  constant as  $|V| \rightarrow \infty$ , which is trivially achieved by imposing

$$|V|/Q = \omega_1, \quad p(Q-1) = \omega_2, \quad (2.19)$$

with  $\omega_1 \gg 1$  and  $\omega_2 > 0$  two independent constants. Each pair  $(\omega_1, \omega_2)$  makes the model approach the thermodynamic limit along a specific trajectory. Universalities, if there are at all, should be defined as invariant properties of the model in the thermodynamic limit with respect to different choices of  $(\omega_1, \omega_2)$ . For later convenience, it is worthwhile defining the fractions

$$\pi_{\text{in}} = \frac{\delta_{\text{in}}}{\delta_{\text{in}} + \delta_{\text{out}}} = \frac{1}{1 + p(Q-1)} = \frac{1}{1 + \omega_2}, \quad (2.20)$$

$$\pi_{\text{out}} = \frac{\delta_{\text{out}}}{\delta_{\text{in}} + \delta_{\text{out}}} = \frac{p(Q-1)}{1 + p(Q-1)} = \frac{\omega_2}{1 + \omega_2}, \quad (2.21)$$

representing the probabilities of intra- and inter-clique interaction, *i.e.* the probabilities that a change of  $\eta(x)$  occurs due to an interaction of  $x$  with a voter belonging to her same clique or to a different one.

### 2.4 Scaling variables

In the thermodynamic limit, the vote vector  $v$  has an increasingly large number of components, each ranging between 0 and  $\omega_1$  (besides contributions from candidates). For this reason, we introduce the normalized variables

$$\phi_k^{(i)} = \frac{Qv_k^{(i)}}{|V|} = \omega_1^{-1}v_k^{(i)}, \quad i, k = 1, \dots, Q. \quad (2.22)$$

In terms of these, eq. (2.16) reads

$$\begin{cases} \sum_{k=1}^Q \phi_k^{(i)}(t) = 1, \\ \phi_i^{(i)}(t) \geq \omega_1^{-1}, \end{cases} \quad i = 1, \dots, Q \quad \text{and} \quad t \in [0, \infty). \quad (2.23)$$

$v_k^{(i)}$	number of votes received by candidate $z_k$ from voters in the $i$ -th clique	
$\phi_k^{(i)} = \omega_1^{-1} v_k^{(i)}$	contribution to the excess of votes of candidate $z_k$ from the $i$ -th clique	eq. (2.22)
$\bar{\phi} = \{\phi_k^{(i)}\}_{i,k:i \neq k}^{1, \dots, Q}$	state vector of the system	
$\mathcal{P}_{\text{VM}}(\bar{\phi})$	probability density of the state vector in the VM	
$\mathcal{P}_{\text{VM}}^{\text{off}}(x)$	marginal probability density of the off-diagonal state variables $\phi_k^{(i)}, i \neq k$	eq. (3.6)
$\mathcal{P}_{\text{VM}}^{\text{diag}}(x)$	marginal probability density of the diagonal state variables $\phi_k^{(k)}$	eq. (3.7)
$\mathcal{F}_{\text{VM}}(x)$	marginal probability density of the excess of votes in the VM	eq. (2.27)
$\mathcal{P}_{\text{FP}}(\bar{\phi})$	probability density of the state vector from the FP equation	eq. (4.9)
$\mathcal{F}_{\text{FP}}(x)$	marginal probability density of the excess of votes from the FP equation	

**Table 1** – Synoptic table of the most relevant quantities considered in the present paper

Thus, we see that the vector  $\phi = \{\phi_k^{(i)}\}_{i,k=1}^Q$  lives on a Cartesian product of cut off simplices

$$\mathcal{T}_Q(\omega_1^{-1}) = T_Q^{(1)}(\omega_1^{-1}) \times \dots \times T_Q^{(Q)}(\omega_1^{-1}), \quad (2.24)$$

$$T_Q^{(i)}(\omega_1^{-1}) = \left\{ x \in \mathbb{R}_+^Q : x_i \geq \omega_1^{-1}, |x|_1 = 1 \right\}, \quad (2.25)$$

with  $|x|_1 = \sum_{k=1}^Q x_k$  the taxicab norm of  $x$ . Owing to the above constraints, vote variables are redundant and one can freely choose to represent one variable per clique in terms of the others. Symmetry suggests to eliminate the diagonal variables  $\phi_k^{(k)}$ . For later convenience, we denote by  $\bar{\phi} = \{\phi_k^{(i)}\}_{i,k:i \neq k}^{1, \dots, Q}$  the vector of the essential variables following our conventional choice. Accordingly, the intra-party excess of votes candidate  $z_k$  receives is given by

$$\phi_k = \sum_{i=1}^Q \phi_k^{(i)} = 1 + \sum_{i \neq k}^{1 \dots Q} \phi_k^{(i)} - \sum_{i \neq k}^{1 \dots Q} \phi_i^{(k)}, \quad k = 1, \dots, Q. \quad (2.26)$$

These are just the scaling variables considered by FC, expressed in the language of cliques. If  $\mathcal{P}_{\text{VM}}(\bar{\phi})$  denotes the probability density of the normalized vote vector at equilibrium, then the probability density of  $\phi_k$  (which is independent of  $k$  as a consequence of the symmetries of the model) is represented by the marginal distribution

$$\mathcal{F}_{\text{VM}}(x) = \int_{\mathcal{T}_Q(\omega_1^{-1})} \delta(\phi_k - x) \mathcal{P}_{\text{VM}}(\bar{\phi}) d\bar{\phi}. \quad (2.27)$$

The reader should bear in mind that in the thermodynamic limit  $\phi_k$  ranges over an infinite set of discrete values, namely  $\phi_k = \omega_1^{-1} \ell$ ,  $\ell = 1, 2, \dots, |V|(1 - \omega_1^{-1})$ . The minimum variation of  $\phi_k$  is thus  $\Delta\phi_k = \omega_1^{-1}$ . When  $\Delta\phi_k \ll \phi_k$  we can legitimately consider  $\phi_k$  as a continuous variable, but close to the lower bound  $\omega_1^{-1}$  the quantization of  $\phi_k$  is unmistakable. Anyway, an exact representation of  $\mathcal{F}_{\text{VM}}(x)$  at all scales should be given in terms of Dirac delta functions, *i.e.*

$$\mathcal{F}_{\text{VM}}(x) = \sum_{\ell=1}^{\infty} c_\ell \delta(x - \omega_1^{-1} \ell), \quad \sum_{\ell=1}^{\infty} c_\ell = 1, \quad (2.28)$$

in the thermodynamic limit.

A summary of the most relevant quantities considered in the present paper is reported in Table 1.

$\omega_1$	$\omega_2$	$ V $	$Q$	$p$	$\omega_1$	$\omega_2$	$ V $	$Q$	$p$
1,000.0	0.3	12,000	12	$2.727273 \times 10^{-2}$	2,000.0	0.3	12,000	6	$6.000000 \times 10^{-2}$
		24,000	24	$1.304348 \times 10^{-2}$			24,000	12	$2.727273 \times 10^{-2}$
		48,000	48	$6.382979 \times 10^{-3}$			48,000	24	$1.304348 \times 10^{-2}$
		72,000	72	$4.225352 \times 10^{-3}$			72,000	36	$8.571429 \times 10^{-3}$
		96,000	96	$3.157895 \times 10^{-3}$			96,000	48	$6.382979 \times 10^{-3}$
1,000.0	0.6	12,000	12	$5.454545 \times 10^{-2}$	2,000.0	0.6	12,000	6	$1.200000 \times 10^{-1}$
		24,000	24	$2.608696 \times 10^{-2}$			24,000	12	$5.454545 \times 10^{-2}$
		48,000	48	$1.276596 \times 10^{-2}$			48,000	24	$2.608696 \times 10^{-2}$
		72,000	72	$8.450704 \times 10^{-3}$			72,000	36	$1.714286 \times 10^{-2}$
		96,000	96	$6.315789 \times 10^{-3}$			96,000	48	$1.276596 \times 10^{-2}$
1,000.0	0.9	12,000	12	$8.181818 \times 10^{-2}$	2,000.0	0.9	12,000	6	$1.800000 \times 10^{-1}$
		24,000	24	$3.913043 \times 10^{-2}$			24,000	12	$8.181818 \times 10^{-2}$
		48,000	48	$1.914894 \times 10^{-2}$			48,000	24	$3.913043 \times 10^{-2}$
		72,000	72	$1.267606 \times 10^{-2}$			72,000	36	$2.571429 \times 10^{-2}$
		96,000	96	$9.473684 \times 10^{-3}$			96,000	48	$1.914894 \times 10^{-2}$

**Table 2** – Parameters for the simulation of the autocorrelation time, the average values of  $\phi_k^{(i)}$  and the distribution  $\mathcal{F}_{\text{VM}}(x)$  of the excess of votes.

### 3 Monte Carlo simulations of the VM

As well known since [22], competing candidates prevent the system from reaching exit configurations. The extremal states  $\phi_k = \omega_1^{-1}$  behave like reflecting boundaries in  $\bar{X}$ . They make the microscopic dynamics of the model run endlessly. After a transient depending on the initial state, the voter configuration reaches a dynamic equilibrium governed by  $\mathcal{P}_{\text{VM}}(\bar{\phi})$ . We explore this numerically by means of Monte Carlo simulations.

In the thermodynamic limit, the parameter space of the model is represented by the pairs  $(\omega_1, \omega_2)$ . At finite  $|V|$  the adjacency matrix becomes denser as  $\omega_1$  and/or  $\omega_2$  increase. Simulations become in this limit more and more demanding, owing to both an increasingly severe memory requirement to host the model on a machine and an intrinsic enhancement of the autocorrelation time, as we discuss in a moment. According to such restrictions and the computing power in our availability, we choose to simulate the model at  $\omega_1 = 1,000.0, 2,000.0$  and  $\omega_2 = 0.3, 0.6, 0.9$ . For each pair  $(\omega_1, \omega_2)$ , we perform simulations at five values of  $|V|$ , so as to be able to observe clearly how the system approaches the thermodynamic limit. Simulation parameters are reported in Table 2. For each set of values, we extract randomly 20 network samples at  $\omega_1 = 1,000.0$  and 40 network samples at  $\omega_1 = 2,000.0$  and average results over them. All simulations start from a random configuration of voters, with political preferences assigned independently with a flat probability of  $1/Q$ .

#### 3.1 Autocorrelation time

As usual in the language of Monte Carlo simulations, we define a sweep as a number  $|V| - Q$  of single-voter updates, so that on average each dynamic voter is updated once in a sweep. The autocorrelation time  $\tau_{\text{VM}}$  measures the average number of sweeps separating two statistically independent voter configurations. In order to simulate  $\tau_{\text{VM}}$ , we proceed as follows. Given two generic configurations  $\eta(\cdot)$  and  $\bar{\eta}(\cdot)$ , we define their overlap  $\langle \eta(\cdot) | \bar{\eta}(\cdot) \rangle$  as the fraction of voters sharing the same political preference, namely

$$\langle \eta(\cdot) | \bar{\eta}(\cdot) \rangle = \frac{1}{|V|} \sum_{x \in V} \delta_{\eta(x), \bar{\eta}(x)}. \quad (3.1)$$

Hence, we define the autocorrelation function as

$$\mathcal{C}(t) = \langle \eta(\cdot, s) | \eta(\cdot, s+t) \rangle. \quad (3.2)$$

At equilibrium,  $\mathcal{C}(t)$  depends upon  $s$  only via statistical fluctuations, which are suppressed by averaging over Markov chains. It should be observed that at finite  $|V|$ ,  $\mathcal{C}(t)$  does not vanish as  $t \rightarrow \infty$ . Indeed, any dynamic voter has a probability  $1/Q$  of expressing the same political preference at times  $s$  and  $s+t$  even though  $\eta(\cdot, s)$  and  $\eta(\cdot, s+t)$  are statistically independent. Since the number of dynamic voters is  $|V| - Q$ , such finite probability gives a contribution of  $(|V| - Q)/|V|Q = (1 - \omega_1^{-1})/Q$  to  $\mathcal{C}(t)$  as  $t \rightarrow \infty$ . An additional contribution of  $Q/|V| = \omega_1^{-1}$  is due to the zealotry of the candidates. Thus, we conclude that

$$\mathcal{C}(t) \underset{t \rightarrow \infty}{\sim} \mathcal{C}_0 + \mathcal{A} \exp\left(-\frac{t}{\tau_{\text{VM}}}\right), \quad \mathcal{C}_0 = \frac{1}{|V|} \left[ Q + \frac{|V| - Q}{Q} \right] = \omega_1^{-1} + \frac{1 - \omega_1^{-1}}{Q}, \quad (3.3)$$

with an appropriate factor  $\mathcal{A}$ , depending on the details of system but not on  $t$ . In particular, we note that  $\mathcal{C}_0 \rightarrow \omega_1^{-1}$  in the thermodynamic limit. In order to extract  $\tau_{\text{VM}}$  from  $\mathcal{C}(t)$ , we introduce the effective autocorrelation time

$$\tau_{\text{eff}}(t) = 1/\log \left\{ \frac{\mathcal{C}(t) - \mathcal{C}_0}{\mathcal{C}(t+1) - \mathcal{C}_0} \right\}. \quad (3.4)$$

From eq. (3.3) it follows that  $\tau_{\text{eff}}(t)$  depends upon  $t$  only via fluctuations. Instead of averaging over several Monte Carlo histories, we extract  $\tau_{\text{VM}}$  from a single Markov chain. An example is shown in Fig. 2 (top). This plot refers to parameters  $(|V|, Q, p) = (48,000, 48, 6.383 \times 10^{-3})$ , corresponding to  $(\omega_1, \omega_2) = (1,000.0, 0.3)$ . It has been obtained according to the following procedure. Starting from a random voter configuration, we let the system relax to the equilibrium: 15,000 sweeps are largely sufficient to this aim. We then reconstruct  $\mathcal{C}(t)$  from the subsequent 35,000 configurations by averaging the overlap of all those, which are separated by a time distance of  $t$ . From  $\mathcal{C}(t)$  we compute  $\tau_{\text{eff}}(t)$  and look at the quartiles  $\mathcal{Q}_k$  ( $k = 1, 2, 3$ ) of the distribution it generates in the range  $t \in [100, 600]$ : larger values of  $t$  can be certainly considered, yet the statistical noise becomes increasingly important. We take  $\tau_{\text{VM}} = \mathcal{Q}_2$  as our best estimate and  $\Delta\tau_{\text{VM}} = \max\{\mathcal{Q}_3 - \mathcal{Q}_2, \mathcal{Q}_2 - \mathcal{Q}_1\}$  as its uncertainty. Numbers depend on the network sample, therefore we average over several networks as explained above. Standard error propagation is applied upon averaging.

Results for  $\tau_{\text{VM}}$  are shown in Fig. 2 (bottom) together with the MFT prediction

$$\tau_{\text{FP}} = \omega_1(1 + \omega_2)(1 - \omega_1^{-1}), \quad (3.5)$$

which is derived in sect. 4. They admit a straightforward interpretation.

- As  $\omega_2 \rightarrow 0$  the long-range competition among candidates reduces and the cliques converge to full consensus, each towards its own candidate. The size of the consensus domains is  $\omega_1$  close to this limit, thus one should expect  $\tau_{\text{VM}} \simeq \omega_1$ . MFT predicts indeed  $\tau_{\text{FP}} \rightarrow \omega_1 - 1$ . Candidates are responsible for the small correction of  $-1$ .
- Upon increasing  $\omega_1$ , the intra-clique consensus domains enlarge independent of  $\omega_2$ , thus making  $\tau_{\text{VM}}$  increase correspondingly.
- The long-range competition among candidates intensifies at larger  $\omega_2$ . The probability of producing consensus domains extending over different cliques increases correspondingly, thus enhancing  $\tau_{\text{VM}}$ .
- The statistical uncertainty on  $\tau_{\text{VM}}$  increases at larger  $\omega_2$ . Since inter-clique interactions intensify as  $\omega_2$  increases and consensus domains are progressively free to spread over different cliques, the variance of the distribution of  $\tau_{\text{eff}}$  along a single Markov chain increases as well.

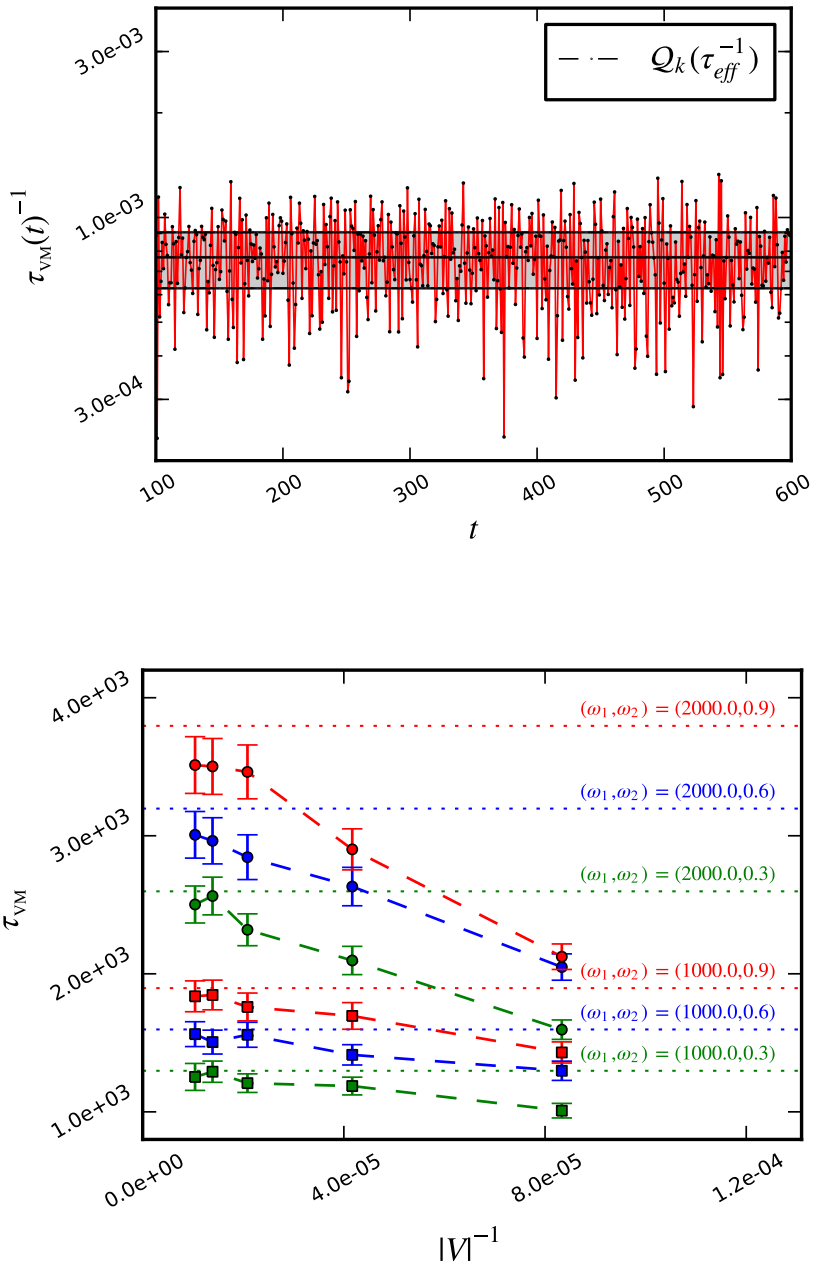


**Figure 2** – *Top*: fluctuations of  $\tau_{eff}(t)^{-1}$  along a single Markov chain at  $(|V|, Q, p) = (48,000, 48, 6.383 \times 10^{-3})$ . *Bottom*: thermodynamic limit of  $\tau_{VM}$  for several values of  $(\omega_1, \omega_2)$ . Horizontal dotted lines correspond to MFT predictions. Finite size effects are compatible with  $O(|V|^{-1})$ -terms.

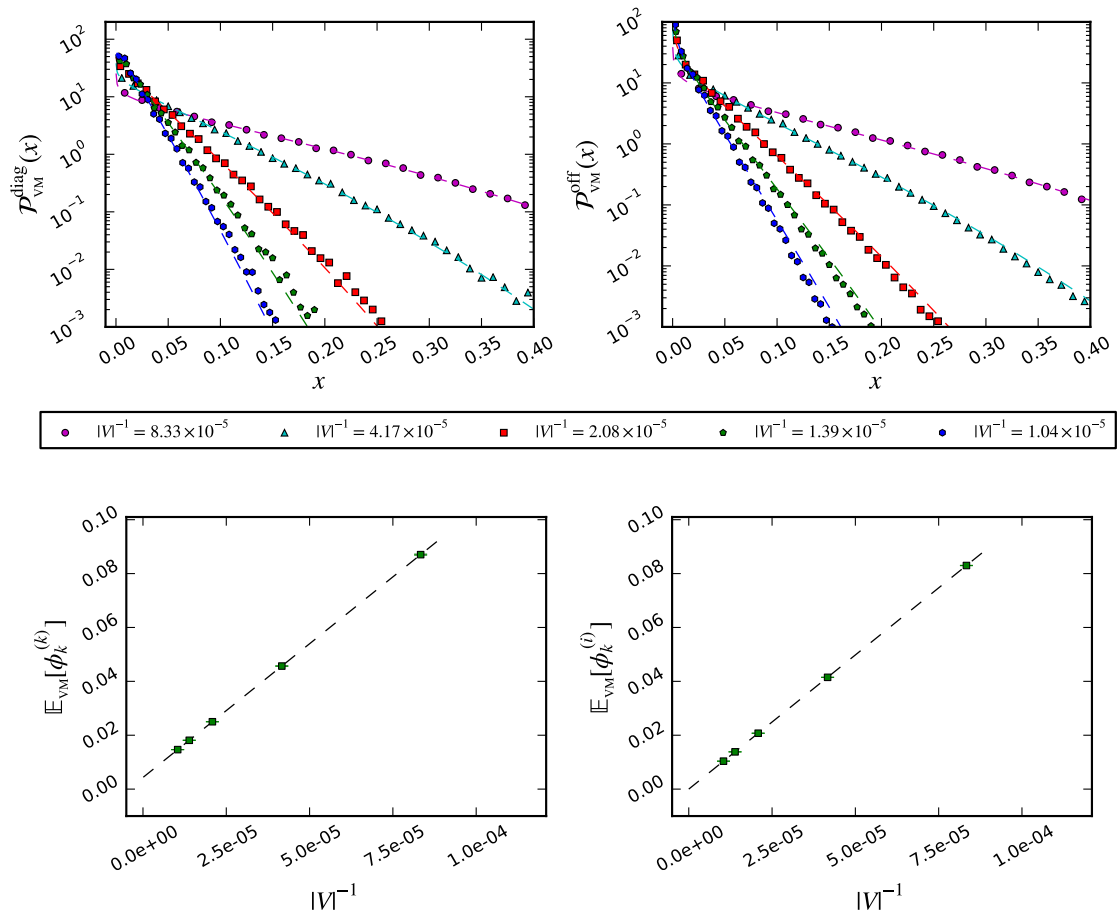


**Figure 3** – *Top*: marginal distribution of the scaling variables at  $(\omega_1, \omega_2) = (1000.0, 0.3)$ . Dashed lines are empirical fits to Beta distributions. *Bottom*: average value of the scaling variables at  $(\omega_1, \omega_2) = (1000.0, 0.3)$ . Dashed lines represent MFT predictions.

We finally observe that the MFT prediction  $\tau_{\text{FP}}$  coincides with  $\mathbb{E}|\text{adj}_V(x)|$  of eq. (2.17). This is not surprising, given the microscopic interaction rule of the VM: it suggests that on average a voter is ready to change political preference just when all her neighbors have changed their minds.

### 3.2 Marginal distributions and average votes

Having estimated the autocorrelation time, we can safely simulate the equilibrium distribution of the VM. Following an initial thermalization, we take a snapshot of the system every  $\Delta t = k\tau_{\text{FP}}$  sweeps, with  $k$  an integer chosen so that  $\exp\{-k\} < 1/Q$ . In this way we ensure that the exponential correlation of eq. (3.3) lies below the threshold  $\mathcal{C}_0$ . For instance, at the largest value of  $Q$  among those reported in Table 2, we set  $k = 5$ . By collecting equally large numbers of voter configurations for each network sample at given parameters  $(|V|, Q, p)$ , we reconstruct the marginal distributions of the scaling variables

$$\mathcal{P}_{\text{VM}}^{\text{off}}(x) = \int_{\mathcal{T}_Q(\omega_1^{-1})} \delta(\phi_k^{(i)} - x) \mathcal{P}_{\text{VM}}(\bar{\phi}) d\bar{\phi}, \quad i \neq k, \quad (3.6)$$

$$\mathcal{P}_{\text{VM}}^{\text{diag}}(x) = \int_{\mathcal{T}_Q(\omega_1^{-1})} \delta\left(1 - \sum_{i \neq k}^{1 \dots Q} \phi_i^{(k)} - x\right) \mathcal{P}_{\text{VM}}(\bar{\phi}) d\bar{\phi}, \quad (3.7)$$

$\omega_1$	$\omega_2$	$Q$	$a_{\text{diag}}$	$b_{\text{diag}}$	$a_{\text{off}}$	$b_{\text{off}}$
1,000.0	0.3	12	$8.28(3) \times 10^{-1}$	$8.70(4) \times 10^0$	$7.543(8) \times 10^{-1}$	$8.33(1) \times 10^0$
		24	$8.67(2) \times 10^{-1}$	$1.811(5) \times 10^1$	$7.178(4) \times 10^{-1}$	$1.658(1) \times 10^1$
		48	$9.45(2) \times 10^{-1}$	$3.687(9) \times 10^1$	$6.647(2) \times 10^{-1}$	$3.138(1) \times 10^1$
		72	$1.017(2) \times 10^0$	$5.51(1) \times 10^1$	$6.194(1) \times 10^{-1}$	$4.417(1) \times 10^1$
		96	$1.079(2) \times 10^0$	$7.25(1) \times 10^1$	$5.820(1) \times 10^{-1}$	$5.553(1) \times 10^1$
1,000.0	0.6	12	$6.74(2) \times 10^{-1}$	$7.19(3) \times 10^0$	$6.351(7) \times 10^{-1}$	$7.005(8) \times 10^0$
		24	$6.87(2) \times 10^{-1}$	$1.488(5) \times 10^1$	$6.082(4) \times 10^{-1}$	$1.403(1) \times 10^1$
		48	$7.32(2) \times 10^{-1}$	$3.056(7) \times 10^1$	$5.797(2) \times 10^{-1}$	$2.732(1) \times 10^1$
		72	$7.72(1) \times 10^{-1}$	$4.664(9) \times 10^1$	$5.580(1) \times 10^{-1}$	$3.973(1) \times 10^1$
		96	$8.31(1) \times 10^{-1}$	$6.29(1) \times 10^1$	$5.394(1) \times 10^{-1}$	$5.138(1) \times 10^1$
1,000.0	0.9	12	$5.73(2) \times 10^{-1}$	$6.16(3) \times 10^0$	$5.453(6) \times 10^{-1}$	$6.011(8) \times 10^0$
		24	$5.73(2) \times 10^{-1}$	$1.257(4) \times 10^1$	$5.203(3) \times 10^{-1}$	$1.200(1) \times 10^1$
		48	$6.00(1) \times 10^{-1}$	$2.565(7) \times 10^1$	$4.970(2) \times 10^{-1}$	$2.341(1) \times 10^1$
		72	$6.46(1) \times 10^{-1}$	$3.983(9) \times 10^1$	$4.891(1) \times 10^{-1}$	$3.481(1) \times 10^1$
		96	$6.81(1) \times 10^{-1}$	$5.38(1) \times 10^1$	$4.752(1) \times 10^{-1}$	$4.524(1) \times 10^1$
2,000.0	0.3	6	$8.67(4) \times 10^{-1}$	$4.29(2) \times 10^0$	$8.49(2) \times 10^{-1}$	$4.25(1) \times 10^0$
		12	$8.18(5) \times 10^{-1}$	$8.78(6) \times 10^0$	$7.81(2) \times 10^{-1}$	$8.61(2) \times 10^0$
		24	$8.33(5) \times 10^{-1}$	$1.82(1) \times 10^1$	$7.58(1) \times 10^{-1}$	$1.747(3) \times 10^1$
		36	$8.43(7) \times 10^{-1}$	$2.74(3) \times 10^1$	$7.27(1) \times 10^{-1}$	$2.550(4) \times 10^1$
		48	$8.64(7) \times 10^{-1}$	$3.68(4) \times 10^1$	$7.12(1) \times 10^{-1}$	$3.352(5) \times 10^1$
2,000.0	0.6	6	$7.18(3) \times 10^{-1}$	$3.57(2) \times 10^0$	$7.09(1) \times 10^{-1}$	$3.55(1) \times 10^0$
		12	$6.55(5) \times 10^{-1}$	$7.10(6) \times 10^0$	$6.35(1) \times 10^{-1}$	$6.70(2) \times 10^0$
		24	$6.62(6) \times 10^{-1}$	$1.48(1) \times 10^1$	$6.21(1) \times 10^{-1}$	$1.430(3) \times 10^1$
		36	$6.78(6) \times 10^{-1}$	$2.27(2) \times 10^1$	$6.16(1) \times 10^{-1}$	$2.159(4) \times 10^1$
		48	$6.83(7) \times 10^{-1}$	$3.02(3) \times 10^1$	$6.02(1) \times 10^{-1}$	$2.833(5) \times 10^1$
2,000.0	0.9	6	$6.19(5) \times 10^{-1}$	$3.08(3) \times 10^0$	$6.11(2) \times 10^{-1}$	$3.06(1) \times 10^0$
		12	$5.72(5) \times 10^{-1}$	$6.21(6) \times 10^0$	$5.57(1) \times 10^{-1}$	$6.14(2) \times 10^0$
		24	$5.59(5) \times 10^{-1}$	$1.26(1) \times 10^1$	$5.32(1) \times 10^{-1}$	$1.224(3) \times 10^1$
		36	$5.65(6) \times 10^{-1}$	$1.91(2) \times 10^1$	$5.22(1) \times 10^{-1}$	$1.829(4) \times 10^1$
		48	$5.70(6) \times 10^{-1}$	$2.55(3) \times 10^1$	$5.15(1) \times 10^{-1}$	$2.422(5) \times 10^1$

**Table 3** – Fit parameters of  $\mathcal{P}_{\text{VM}}^{\text{diag}}$  and  $\mathcal{P}_{\text{VM}}^{\text{off}}$  vs.  $\beta_{a,b}(x)$ .

and their expectations

$$\mathbb{E}_{\text{VM}}[\phi_k^{(i)}] = \int_0^{1-\omega_1^{-1}} dx x \mathcal{P}_{\text{VM}}^{\text{off}}(x), \quad i \neq k, \quad (3.8)$$

$$\mathbb{E}_{\text{VM}}[\phi_k^{(k)}] = \int_{\omega_1^{-1}}^1 dx x \mathcal{P}_{\text{VM}}^{\text{diag}}(x). \quad (3.9)$$

In Fig. 3 (top) we show  $\mathcal{P}_{\text{VM}}^{\text{diag}}$  and  $\mathcal{P}_{\text{VM}}^{\text{off}}$  at  $(\omega_1, \omega_2) = (1,000.0, 0.3)$ . Points represent results of the Monte Carlo simulations, while curves correspond to empirical fits to Beta distributions

$$\beta_{a,b}(x) = \frac{\Gamma(a+b)}{\Gamma(a)\Gamma(b)} x^{a-1} (1-x)^{b-1}. \quad (3.10)$$

The fit constants  $a$  and  $b$ , used in the plot and reported in Table 3 for all sets of simulation parameters, have been obtained by comparing the numerical estimates of mean and variance with the corresponding

analytic expressions known for the Beta distribution, namely

$$\mathbb{E}_{a,b}[x] = \frac{a}{a+b}, \quad \text{var}_{a,b}[x] = \frac{ab}{(a+b)^2(a+b+1)}. \quad (3.11)$$

The uncertainties quoted in Table 3 have been obtained by bootstrapping distributions from those simulated. The interpolation looks overall rather precise, though its quality worsens slightly at the largest values of  $|V|$ . In the thermodynamic limit the marginal distributions are indeed squeezed towards increasingly small values of the scaling variables, where quantization effects become non-negligible. At such low scales, any *ansatz* based on a continuous density is intrinsically unsuitable to describe the numerical data. The reader will certainly notice that the fit parameters are far from being uncorrelated. A close inspection to Table 3 suggests indeed the approximate distributional laws

$$\mathcal{P}_{\text{VM}}^{\text{off}}(x) \approx \beta_{\alpha, \bar{\alpha} + (Q-2)\alpha}(x), \quad (3.12)$$

$$\mathcal{P}_{\text{VM}}^{\text{diag}}(x) \approx \beta_{\bar{\alpha}, (Q-1)\alpha}(x), \quad (3.13)$$

with  $\alpha = \alpha(\omega_1, \omega_2, |V|)$  and  $\bar{\alpha} = \bar{\alpha}(\omega_1, \omega_2, |V|)$  being characterized by a residual dependence on  $|V|$ , which is difficult to assess. We shall come back to eqs. (3.12)–(3.13) in Appendix A. For the moment, we just observe that, regardless of the analytic form of the distributions, diagonal and off-diagonal scaling variables look very similar, though they are not marginally identical. This makes us conclude that candidates do not exert a very strong influence on their clique mates at the simulation parameters considered. Nevertheless, the difference among  $\phi_k^{(i)}$  and  $\phi_k^{(k)}$  increases as  $|V| \rightarrow \infty$ . To check this, in Fig 3 (bottom) we plot the average values of the scaling variables at  $(\omega_1, \omega_2) = (1,000.0, 0.3)$  vs. the prediction of MFT

$$\mathbb{E}_{\text{FP}}[\phi_k^{(i)}] = \frac{\delta_{ik} [Q - 1 + \omega_2 Q (1 - \omega_1^{-1})] + \omega_1 \omega_2 (1 - \omega_1^{-1})^2}{Q - 1 + \omega_1 \omega_2 Q (1 - \omega_1^{-1})}, \quad (3.14)$$

which is derived again in sect. 4. The agreement is very good. Moreover, we see that  $\mathbb{E}_{\text{FP}}[\phi_k^{(i)}]$  vanishes in the thermodynamic limit for  $i \neq k$ , while it keeps finite for  $i = k$ . The reason is that in this limit the vector  $\phi$  includes just one diagonal component per clique and an infinite number of off-diagonal ones.

### 3.3 Distribution of the excess of votes

In Fig. 4, we show the distribution of the intra-party excess of votes at all parameters of Table 2. As mentioned in sect. 1, plots resemble roughly the distribution observed in the real Brazilian elections. A few considerations are due.

- We notice at first glance that the dependence of the distributions upon  $|V|$  is minimal:  $\mathcal{F}_{\text{VM}}(x)$  is very close to the thermodynamic limit at all simulation parameters. Finite size effects are only visible along the right tails. This is in clear contrast with the substantial dependence upon  $|V|$  displayed by the marginal distributions. Although the model bears the FC scaling formally just in the thermodynamic limit, in practice  $\mathcal{F}_{\text{VM}}(x)$  scales very well also at finite  $|V|$ .
- The reader should be aware that the final lift of the left tails is fake. We have already observed in sect. 2.4 that  $\phi_k$  is a discrete variable. Its quantization cannot be neglected at scales comparable to  $\omega_1^{-1}$ . In this region, a representation of  $\mathcal{F}_{\text{VM}}(x)$  as a histogram is meaningless, as the number of events falling within any bin (surrounding a Dirac delta) is independent of the bin size, while the height of the corresponding rectangle is proportionally inverse to it. The histogram becomes stable at  $\phi_k \gtrsim 5\omega_1^{-1}$ , thus the last three to four points on the left should be ignored. We show them in Fig. 4 purposely to highlight the phenomenon.

- The central part of the distribution follows a power law  $\mathcal{F}_{\text{VM}}(x) \propto x^{-\alpha}$ , with  $\alpha$  depending on the model parameters. In particular,  $\alpha$  increases with  $\omega_2$ .
- Unfortunately, the right tail of  $\mathcal{F}_{\text{VM}}(x)$  is not log-normal, at least at the simulation parameters of Table 2. Since the distribution of the Brazilian data fits very well the FC universal curve at  $x \gtrsim 1$  (as pointed out in [2]), this appears to be a clear point of phenomenological weakness of our model.
- Establishing how  $\mathcal{F}_{\text{VM}}(x)$  depends upon  $(\omega_1, \omega_2)$  is non-trivial. It would be tempting to introduce renormalization group concepts by investigating whether  $\mathcal{F}_{\text{VM}}(x)$  is invariant along some trajectory  $(\omega_1, \omega_2(\omega_1))$ , but simulations are CPU demanding and we have not explored this possibility yet.

In conclusion, upon evaluating the phenomenological valence of the model it should be certainly kept in mind that  $\mathcal{F}_{\text{VM}}(x)$  depends on just two parameters, so the model should be just taken as a rough prototype of more sophisticated (and realistic) constructions. Moreover,  $\mathcal{F}_{\text{VM}}(x)$  is in a sense a pure state distribution, in that it does not mix different values of  $(\omega_1, \omega_2)$ .

## 4 Clique MFT

Besides numerical simulations, MFT represents the simplest approach to studying birth–death models such as the VM. Its main benefit is the possibility of investigating the system in analytic terms. Although the Fokker–Planck equation of the model cannot be solved exactly (as we shall see below), it holds approximate information on the fluctuations of  $\bar{\phi}$ , on the dependence of  $\mathcal{P}_{\text{VM}}$  upon the network topology, on the influence exerted by each candidate on her own clique and the others and on how the competition between candidates leads to the specific equilibrium discussed in the previous section. Therefore, looking at the MFT of the model represents a necessary step towards a full understanding of the distribution of the excess of votes.

In the framework of MFT, the system is described in terms of macroscopic states and its probability density follows from a Master Equation. The defining feature of MFT is the observation of the microscopic dynamics from a distance comparable to the size of the system. At this length scale, transition rates are obtained by counting over the whole network the agents, who are potentially responsible for the variation of macroscopic variables in a given state. This approach is pursued in [22] for the binary VM with zealots and in [10] for the multi-state VM with no zealots. Its main drawback is that overall transition rates bring no information about the topological details of the network. Thus, MFT fails to describe the system whenever topology plays an essential rôle in the microscopic dynamics.

In the context of the model introduced in sect. 2, cliques are the leading topological structures. Accordingly, it makes sense to increase the resolving power of MFT by observing the microscopic dynamics from a distance comparable to the size of a clique. To this aim, we observe that a single event where the vote of  $x \in V_0$  switches from  $m$  to  $\ell$ , occurs nowhere but the clique  $C_i \ni x$ . The transition turns the vote vector  $v$  into a new one  $v_{\ell^+ m^-}^{(i)}$  with components

$$\left(v_{\ell^+ m^-}^{(i)}\right)_s^{(r)} = \begin{cases} v_s^{(i)} + 1, & \text{if } r = i, \quad s = \ell; \\ v_s^{(i)} - 1, & \text{if } r = i, \quad s = m; \\ v_s^{(i)}, & \text{if } r = i, \quad s \neq \ell, m; \\ v_s^{(r)}, & \text{if } r \neq i, \quad s = 1, \dots, Q. \end{cases} \quad (4.1)$$

At this length scale the Master Equation reads

$$\partial_t \mathcal{P}(v) = \frac{1}{2} \sum_{i=1}^Q \sum_{\ell \neq m}^{1 \dots Q} \left[ w(v | v_{\ell^+ m^-}^{(i)}) \mathcal{P}(v_{\ell^+ m^-}^{(i)}) - w(v_{\ell^+ m^-}^{(i)} | v) \mathcal{P}(v) \right], \quad (4.2)$$

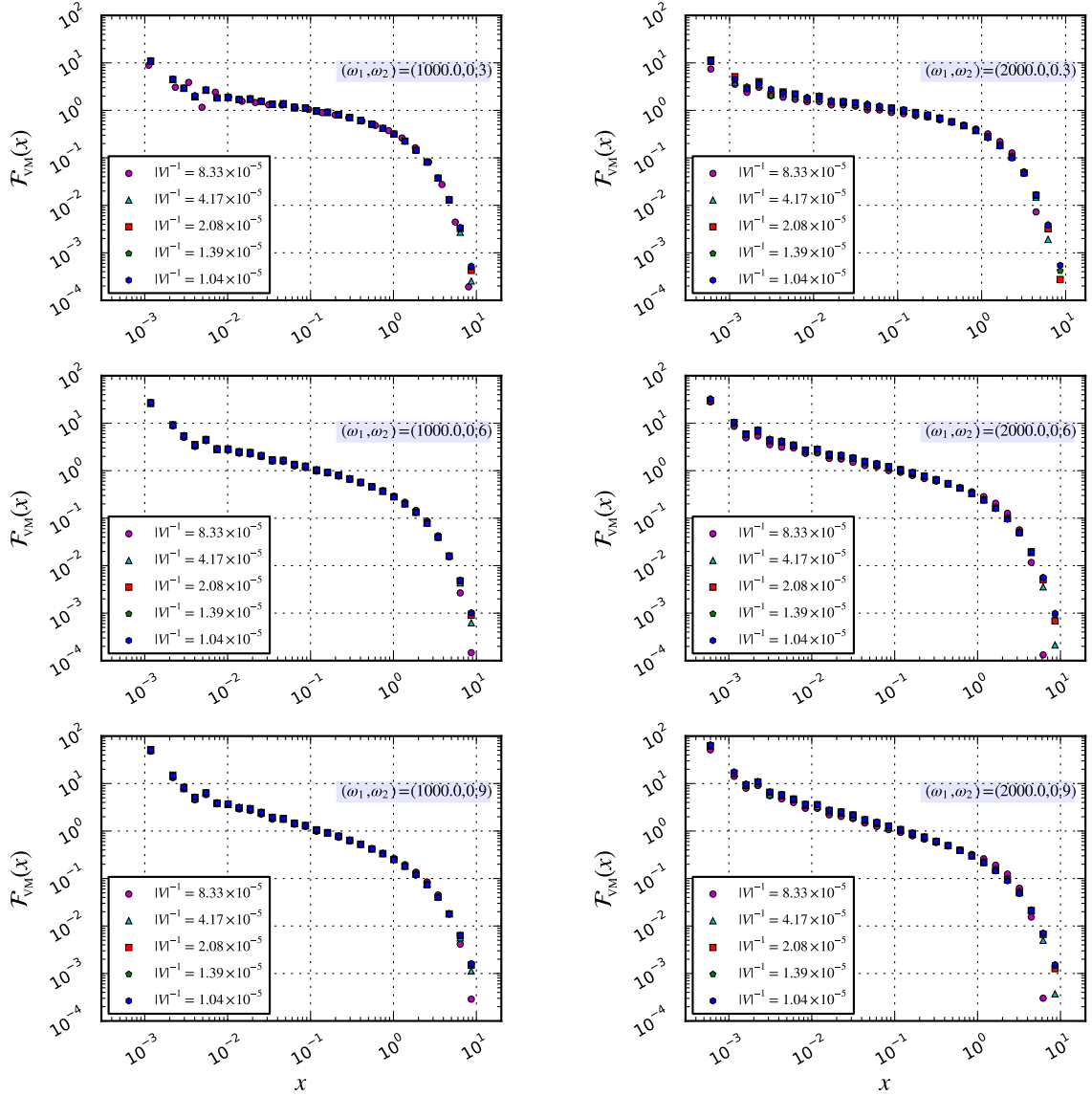


**Figure 4** – Distribution of the intra-party excess of votes.

where  $\partial_t = \partial/\partial t$  and  $w(v_{\ell+m}^{(i)}|v)$  measures the rate of the transition  $v \rightarrow v_{\ell+m}^{(i)}$ . We then notice that  $w$  is made of two contributions, describing events due to intra- and inter-clique interactions. Specifically, we have

$$w(v_{\ell+m}^{(i)}|v) = \frac{1}{\Delta t} \frac{v_m^{(i)} - \delta_{mi}}{|V| - 1} \left[ \pi_{\text{in}} \frac{v_{\ell}^{(i)}}{|V| - 1} + \frac{\pi_{\text{out}}}{Q-1} \sum_{k \neq i}^{1 \dots Q} \frac{v_{\ell}^{(k)} - \delta_{kl}}{|V| - 1} \right], \quad (4.3)$$

$$w(v|v_{\ell+m}^{(i)}) = \frac{1}{\Delta t} \frac{v_{\ell}^{(i)} + 1 - \delta_{\ell i}}{|V| - 1} \left[ \pi_{\text{in}} \frac{v_m^{(i)} - 1}{|V| - 1} + \frac{\pi_{\text{out}}}{Q-1} \sum_{k \neq i}^{1 \dots Q} \frac{v_m^{(k)} - 1 - \delta_{km}}{|V| - 1} \right]. \quad (4.4)$$

To check the above expressions, the reader should keep in mind that: *i*) the only agents experiencing

transitions are those in  $V_0$ ; *ii*) candidates participate in the microscopic dynamics as opinion donors; *iii*) candidates do not take part in inter-clique interactions.

It should be also observed that, since we measure time in units of sweeps, an elementary transition occurs on average in a time interval  $\delta t = (|V| - Q)^{-1}$ . Since the network is made of  $Q$  cliques, a transition within a specific one occurs on average in a time interval which is larger than  $\delta t$  by a factor of  $Q$ . Accordingly, we set  $\Delta t = Q\delta t = Q/(|V| - Q) = 1/\delta_{\text{in}}$ .

Thanks to the definitions introduced in eq. (2.18), eqs. (4.3)–(4.4) simplify to

$$w\left(v_{\ell+m^-}^{(i)}|v\right) = \left(v_m^{(i)} - \delta_{mi}\right) \left[ \frac{\pi_{\text{in}}}{\delta_{\text{in}}} v_\ell^{(i)} + p \frac{\pi_{\text{out}}}{\delta_{\text{out}}} \sum_{k \neq i}^{1\dots Q} (v_\ell^{(k)} - \delta_{k\ell}) \right], \quad (4.5)$$

$$w\left(v|v_{\ell+m^-}^{(i)}\right) = \left(v_\ell^{(i)} + 1 - \delta_{\ell i}\right) \left[ \frac{\pi_{\text{in}}}{\delta_{\text{in}}} (v_m^{(i)} - 1) + p \frac{\pi_{\text{out}}}{\delta_{\text{out}}} \sum_{k \neq i}^{1\dots Q} (v_m^{(k)} - 1 - \delta_{km}) \right]. \quad (4.6)$$

## 4.1 Kramers–Moyal expansion

Seldom can the Master Equation be solved analytically. Indeed, eq. (4.2) is of no exception. An approximation to it can be obtained by means of the Kramers–Moyal expansion, which upon truncation to second order yields the FP equation (see for instance ch. 7 of [20]). To work out the approximation, we preliminarily express the transition rates in terms of the scaling variables and then expand eq. (4.2) in Taylor series at the target point  $\bar{\phi}$ , where we wish to calculate the probability density. It is worth noticing some subtleties:

- The expansion parameter is identified here with the minimum variation of  $\phi_k^{(i)}$ , namely  $\Delta\phi_k^{(i)} = \omega_1^{-1}$ , while in [10, 22] it is given by  $|V|^{-1}$ . In the thermodynamic limit the former stays finite whereas the latter vanishes. Therefore, the Kramers–Moyal expansion we perform in this paper is somewhat different than in standard MFT. Anyway, the Taylor series is expected to converge rapidly, provided  $\omega_1 \gg 1$ .
- Differentiating the probability density with respect to  $\phi_k^{(i)}$  is only possible provided the latter is assumed to be a continuous variable. Such assumption is certainly correct at  $\phi_k^{(i)} \gg \omega_1^{-1}$ , while it fails miserably close to the quantization scale. For this reason, we expect that distributions obtained from the FP equation deviate from the VM at scales comparable to  $\omega_1^{-1}$ .
- In the thermodynamic limit, it holds  $\Delta t = (\omega_1 - 1)^{-1}$ . Thus, we see that time is also quantized. Nevertheless, we treat time as a continuous variable under the assumption  $\omega_1 \gg 1$ .

Having said that, a simple rescaling of the transition rates yields

$$\tilde{w}\left(\phi_{\ell+m^-}^{(i)}|\phi\right) = \omega_1 \frac{\phi_m^{(i)} - \omega_1^{-1}\delta_{mi}}{(1 - \omega_1^{-1})(1 + \omega_2)} \left[ \phi_\ell^{(i)} + \frac{\omega_2}{Q-1} \sum_{k \neq i}^{1\dots Q} (\phi_\ell^{(k)} - \omega_1^{-1}\delta_{k\ell}) \right], \quad (4.7)$$

$$\tilde{w}\left(\phi|\phi_{\ell+m^-}^{(i)}\right) = \omega_1 \frac{\phi_\ell^{(i)} + \omega_1^{-1}(1 - \delta_{\ell i})}{(1 - \omega_1^{-1})(1 + \omega_2)} \left[ \phi_m^{(i)} - \omega_1^{-1} + \frac{\omega_2}{Q-1} \sum_{k \neq i}^{1\dots Q} (\phi_m^{(k)} - \omega_1^{-1}(1 + \delta_{km})) \right], \quad (4.8)$$

with  $\tilde{w}\left(\phi_{\ell+m^-}^{(i)}|\phi\right) \equiv w\left(v_{\ell+m^-}^{(i)}|v\right)$ . The result of the Kramers–Moyal expansion is the FP equation

$$\partial_t \mathcal{P}_{\text{FP}}(\bar{\phi}) = - \sum_{i=1}^Q \sum_{\ell \neq i}^{1\dots Q} \partial_\ell^{(i)} \left[ A_\ell^{(i)}(\bar{\phi}) \mathcal{P}_{\text{FP}}(\bar{\phi}) \right] + \frac{1}{2} \sum_{i,j=1}^Q \sum_{\ell, m \neq i}^{1\dots Q} \partial_\ell^{(i)} \partial_m^{(j)} \left[ B_{\ell m}^{(ij)}(\bar{\phi}) \mathcal{P}_{\text{FP}}(\bar{\phi}) \right], \quad (4.9)$$

where  $\partial_\ell^{(i)} = \partial/\partial\phi_\ell^{(i)}$ . Not surprisingly, the analytic structure of eq. (4.9) reflects the specific topology of the network. The coefficient functions  $A_\ell^{(i)}$  and  $B_{\ell m}^{(ij)}$  depend on the transition rates via the standard formulae

$$A_\ell^{(i)} = \frac{1}{2} \sum_{k=1}^Q \sum_{a \neq b}^{1 \dots Q} r \left( \phi \rightarrow \phi_{a+b}^{(k)} \right)_\ell^{(i)} \alpha_{a+b}^{(k)}, \quad (4.10)$$

$$B_{\ell m}^{(ij)} = \frac{1}{2} \sum_{k=1}^Q \sum_{a \neq b}^{1 \dots Q} r \left( \phi \rightarrow \phi_{a+b}^{(k)} \right)_\ell^{(i)} r \left( \phi \rightarrow \phi_{a+b}^{(k)} \right)_m^{(j)} \beta_{a+b}^{(k)}, \quad (4.11)$$

with

$$\alpha_{a+b}^{(k)} = \tilde{w} \left( \phi_{a+b}^{(i)} | \phi \right) - \tilde{w} \left( \phi_{a-b}^{(i)} | \phi \right), \quad (4.12)$$

$$\beta_{a+b}^{(k)} = \tilde{w} \left( \phi_{a+b}^{(i)} | \phi \right) + \tilde{w} \left( \phi_{a-b}^{(i)} | \phi \right), \quad (4.13)$$

and

$$r \left( \phi \rightarrow \phi_{a+b}^{(k)} \right)_\ell^{(i)} = \frac{\delta_{ki}}{\omega_1} (\delta_{\ell a} - \delta_{\ell b}). \quad (4.14)$$

Owing to the symmetries  $\alpha_{a+b}^{(k)} = -\alpha_{b+a}^{(k)}$  and  $\beta_{a+b}^{(k)} = \beta_{b+a}^{(k)}$ , the above expressions can be brought to the simplified form

$$A_\ell^{(i)} = \frac{1}{\omega_1} \sum_{a \neq \ell}^{1 \dots Q} \alpha_{\ell+a}^{(i)}, \quad (4.15)$$

$$B_{\ell m}^{(ij)} = \frac{\delta_{ij}}{\omega_1^2} \left[ \delta_{\ell m} \sum_{a \neq \ell}^{1 \dots Q} \beta_{\ell+a}^{(i)} - (1 - \delta_{\ell m}) \beta_{\ell+m}^{(i)} \right] \equiv \delta_{ij} B_{\ell m}^{(i)}. \quad (4.16)$$

We thus see that  $B_{\ell m}^{(ij)}$  is diagonal with respect to the clique indices  $(ij)$ . Yet, we shall show in a moment that  $B_{\ell m}^{(i)}$  depends upon all the components of  $\bar{\phi}$  and not just on  $\{\phi_k^{(i)}\}_{k \neq i}$ . In addition we see that  $B_{\ell m}^{(i)}$  is symmetric with respect to the indices  $(\ell m)$ . Consequently,  $\mathcal{P}_{\text{FP}}(\bar{\phi})$  is invariant under the transformations

$$\text{intra-clique symmetry:} \quad \phi_\ell^{(i)} \longleftrightarrow \phi_m^{(i)}, \quad i = 1, \dots, Q, \quad \ell, m \neq i, \quad (4.17)$$

$$\text{inter-clique symmetry:} \quad \{\phi_k^{(i)}\}_{k \neq i}^{1 \dots Q} \longleftrightarrow \{\phi_k^{(j)}\}_{k \neq j}^{1 \dots Q}, \quad i, j = 1, \dots, Q. \quad (4.18)$$

We finally observe that at equilibrium eq. (4.9) amounts to the local conservation law

$$0 = \sum_{i=1}^Q \sum_{\ell \neq i}^{1 \dots Q} \partial_\ell^{(i)} J_\ell^{(i)}(\bar{\phi}), \quad (4.19)$$

with the vector current  $J_\ell^{(i)}(\bar{\phi})$  given by

$$J_\ell^{(i)}(\bar{\phi}) = A_\ell^{(i)}(\bar{\phi}) \mathcal{P}_{\text{FP}}(\bar{\phi}) - \frac{1}{2} \sum_{m \neq i}^{1 \dots Q} \partial_m^{(i)} \left[ B_{\ell m}^{(i)}(\bar{\phi}) \mathcal{P}_{\text{FP}}(\bar{\phi}) \right]. \quad (4.20)$$

In the context of the binary VM with zealots [22], an exact solution of the FP equation has been obtained by just using the conserved current and a proportionality relation between the coefficient functions. In the present case, proceeding along the same lines looks rather hard. Indeed, since the problem has more than one independent variable, eq. (4.19) does not entail  $J_\ell^{(i)} = \text{const}$ . In addition, the relation between

$A_\ell^{(i)}$  and  $B_{\ell m}^{(i)}$  is more complicated. Yet, we cannot exclude that smart tricks, which unfortunately we have not been able to find, do exist to solve the FP equation analytically.

It takes one page of scratch paper to work out the coefficient functions. A convenient representation, easy to implement on a computer, is given by

$$\begin{aligned} \tau_{\text{FP}} A_\ell^{(i)} = & - [1 + \omega_1 \omega_2 (1 - \omega_1^{-1})] \phi_\ell^{(i)} + \frac{\omega_1 \omega_2 (1 - \omega_1^{-1})}{Q - 1} \left\{ \sum_{k \neq i, \ell}^{1 \dots Q} \phi_\ell^{(k)} - \sum_{k \neq \ell}^{1 \dots Q} \phi_k^{(\ell)} \right\} \\ & + \frac{\omega_1 \omega_2 (1 - \omega_1^{-1})^2}{Q - 1}, \end{aligned} \quad (4.21)$$

$$\begin{aligned} \tau_{\text{FP}} B_{\ell m}^{(i)} = & -2(1 - \delta_{\ell m}) \phi_\ell^{(i)} \phi_m^{(i)} - (1 - \delta_{\ell m}) \frac{\omega_2}{(Q - 1)} \left[ \phi_\ell^{(i)} \left( 1 - \omega_1^{-1} + \sum_{k \neq i, m}^{1 \dots Q} \phi_m^{(k)} - \sum_{k \neq m}^{1 \dots Q} \phi_k^{(m)} \right) \right. \\ & \left. + \phi_m^{(i)} \left( 1 - \omega_1^{-1} + \sum_{k \neq i, \ell}^{1 \dots Q} \phi_\ell^{(k)} - \sum_{k \neq \ell}^{1 \dots Q} \phi_k^{(\ell)} \right) \right] \\ & + 2\delta_{\ell m} \phi_\ell^{(i)} \left[ 1 + \frac{\omega_2 (1 - \omega_1^{-1}) - \omega_1^{-1}}{2} - \phi_\ell^{(i)} \right] \\ & + \delta_{\ell m} \frac{\omega_2}{(Q - 1)} \left( 1 - \omega_1^{-1} - 2\phi_\ell^{(i)} \right) \left[ 1 - \omega_1^{-1} + \sum_{k \neq i, \ell}^{1 \dots Q} \phi_\ell^{(k)} - \sum_{k \neq \ell}^{1 \dots Q} \phi_k^{(\ell)} \right], \quad \ell, m \neq i, \end{aligned} \quad (4.22)$$

with  $\tau_{\text{FP}}$  having been defined in eq. (3.4). We see that as  $\omega_1 \rightarrow \infty$  and  $\omega_2 \rightarrow 0$ , the diffusive coefficient function collapses to the expression found in [10]. The fate of the drift term in the same limit depends on the behavior of the product  $\omega_1 \omega_2$ .

## 4.2 Autocorrelation time and average values from clique MFT

The drift equation obtained by deleting the diffusion term in eq. (4.9) is equivalent to a system of coupled linear differential equations,

$$\frac{d\varphi_\ell^{(i)}}{dt} = A_\ell^{(i)}(\bar{\varphi}), \quad (4.23)$$

with  $\varphi_\ell^{(i)} = \mathbb{E}_{\text{FP}}[\phi_\ell^{(i)}]$ . The expression given in eq. (4.21) for the drift coefficient has been obtained upon applying the simplex constraints, thus it assumes  $\ell \neq i$ . A more general expression, less compact but valid with no restrictions, is

$$\begin{aligned} \tau_{\text{FP}} A_\ell^{(i)}(\bar{\varphi}) = & \sum_{m \neq \ell}^{1 \dots Q} \left( \delta_{\ell i} \varphi_m^{(i)} - \delta_{m i} \varphi_\ell^{(i)} \right) \\ & + \frac{\omega_1 \omega_2}{Q - 1} \sum_{m \neq \ell}^{1 \dots Q} \sum_{k \neq i}^{1 \dots Q} \left[ (\varphi_m^{(i)} - \omega_1^{-1} \delta_{m i}) (\varphi_\ell^{(k)} - \omega_1^{-1} \delta_{k \ell}) - (\varphi_\ell^{(i)} - \omega_1^{-1} \delta_{\ell i}) (\varphi_m^{(k)} - \omega_1^{-1} \delta_{k m}) \right]. \end{aligned} \quad (4.24)$$

We note that the term in square brackets on the second line is antisymmetric in the clique indices  $i, k$ . Upon summing both sides of eq. (4.23) over  $i$ , that term averages to zero. By using the identities  $\sum_{m \neq \ell} \delta_{m i} = (1 - \delta_{\ell i})$  and  $\sum_{m \neq \ell} \varphi_m^{(i)} = 1 - \varphi_\ell^{(i)}$ , we obtain

$$\tau_{\text{FP}} \frac{d\varphi_\ell}{dt} = (1 - \varphi_\ell). \quad (4.25)$$

This equation is trivially solved by the function

$$\varphi_\ell(t) = 1 + (\varphi_\ell(0) - 1)e^{-t/\tau_{\text{FP}}}. \quad (4.26)$$

Since the analytic form of  $\varphi_\ell(t)$  is now known, we can use  $\sum_{k \neq i} \varphi_\ell^{(k)}(t) = \varphi_\ell(t) - \varphi_\ell^{(i)}(t)$  to reduce all terms of eq. (4.23) to functions of the unknown  $\varphi_\ell^{(i)}(t)$  alone. A little algebra yields

$$\tau_{\text{FP}} \frac{d\varphi_\ell^{(i)}}{dt} = \alpha\varphi_\ell - \beta\varphi_\ell^{(i)} + \gamma_{i\ell}, \quad (4.27)$$

with

$$\alpha = \frac{\omega_2(\omega_1 - 1)}{Q - 1}, \quad (4.28)$$

$$\beta = 1 + \omega_2(\omega_1 - 1)\frac{Q}{Q - 1}, \quad (4.29)$$

$$\gamma_{i\ell} = \delta_{i\ell} \left[ 1 + \omega_2(1 - \omega_1^{-1})\frac{Q}{Q - 1} \right] - \frac{\omega_2(1 - \omega_1^{-1})}{Q - 1}. \quad (4.30)$$

Eq. (4.27) can be integrated exactly. The trick to do that is to multiply both sides of it by the integrating factor  $\exp(\beta t/\tau_{\text{FP}})$  and to observe that

$$\tau_{\text{FP}} e^{\beta t/\tau_{\text{FP}}} \frac{d\varphi_\ell^{(i)}}{dt} = \tau_{\text{FP}} \frac{d}{dt} \left( e^{\beta t/\tau_{\text{FP}}} \varphi_\ell^{(i)} \right) - \beta e^{\beta t/\tau_{\text{FP}}} \varphi_\ell^{(i)}. \quad (4.31)$$

Since the indefinite integral of  $\varphi_\ell(t)$  is known, the solution to eq. (4.27) is given by

$$\varphi_\ell^{(i)}(t) = e^{-\beta t/\tau_{\text{FP}}} \varphi_\ell^{(i)}(0) + \frac{\alpha + \gamma_{i\ell}}{\beta} \left( 1 - e^{-\beta t/\tau_{\text{FP}}} \right) + \frac{\alpha [\varphi_\ell(0) - 1]}{\beta - 1} \left( e^{-t/\tau_{\text{FP}}} - e^{-\beta t/\tau_{\text{FP}}} \right). \quad (4.32)$$

We observe that  $\beta \gg 1$  at all simulation parameters of Table 2. Therefore, the time evolution of the average variables is dominated by two largely separated time scales.  $\tau_{\text{FP}}$  is the slowest mode: it governs the relaxation to equilibrium of the averages or — equivalently — the autocorrelation time of the model. In particular, we have

$$\lim_{t \rightarrow \infty} \varphi_\ell^{(i)}(t) = \frac{\alpha + \gamma_{i\ell}}{\beta} = \frac{\delta_{i\ell} [Q - 1 + \omega_2 Q (1 - \omega_1^{-1})] + \omega_1 \omega_2 (1 - \omega_1^{-1})^2}{Q - 1 + \omega_1 \omega_2 Q (1 - \omega_1^{-1})}, \quad (4.33)$$

and

$$\lim_{|V| \rightarrow \infty} \lim_{t \rightarrow \infty} \varphi_i^{(i)}(t) = \frac{1 + \omega_2(1 - \omega_1^{-1})}{1 + \omega_1 \omega_2(1 - \omega_1^{-1})} \equiv \varphi_{\text{diag}}(\omega_1, \omega_2), \quad (4.34)$$

$$\lim_{|V| \rightarrow \infty} \lim_{t \rightarrow \infty} (Q - 1) \varphi_\ell^{(i)}(t) \Big|_{i \neq \ell} = \frac{\omega_1 \omega_2 (1 - \omega_1^{-1})^2}{1 + \omega_1 \omega_2 (1 - \omega_1^{-1})} \equiv \varphi_{\text{off-diag}}(\omega_1, \omega_2). \quad (4.35)$$

Obviously,  $\varphi_{\text{diag}} + \varphi_{\text{off-diag}} = 1$ .

## 5 Numerical integration of the FP equation

It is well known that a multidimensional FP equation with probability density confined within a convex domain  $\mathcal{D}$  is equivalent to a set of coupled stochastic differential equations with reflecting boundary conditions (b.c.) on  $\partial\mathcal{D}$ . In the specific case of eq. (4.9) with b.c.  $\mathcal{P}_{\text{FP}}(\bar{\phi}) = 0$  if  $\phi \notin \mathcal{T}_Q(\omega_1^{-1})$ , the equivalent stochastic process is given by

$$d\phi_\ell^{(i)}(t) = A_\ell^{(i)}(\bar{\phi}) dt + \sum_{k \neq i}^{1 \dots Q} C_{\ell k}^{(i)}(\bar{\phi}) dW_k^{(i)}(t) + dK_\ell^{(i)}(t), \quad i = 1, \dots, Q, \quad \ell \neq i. \quad (5.1)$$

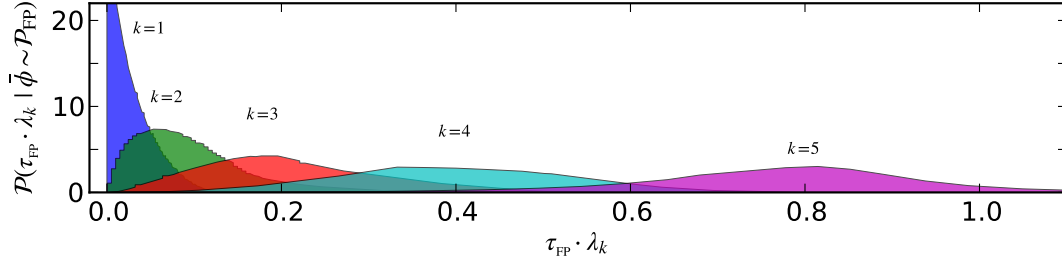


**Figure 5** – Probability density of the ordered eigenvalue spectrum of  $B^{(i)}$  conditioned to  $\bar{\phi} \sim \mathcal{P}_{\text{FP}}$  at  $(\omega_1, \omega_2) = (2,000.0, 0.3)$  and  $Q = 6$ , as obtained from numerically integrating eq. (5.1).

with the matrix  $C_{\ell k}^{(i)}$  being related to  $B_{\ell k}^{(i)}$  via

$$B^{(i)}(\bar{\phi}) = C^{(i)}(\bar{\phi}) \cdot [C^{(i)}(\bar{\phi})]^T. \quad (5.2)$$

As usual,  $W(t) = \{W_k^{(i)}(t)\}_{i \neq k}^{1 \dots Q}$  is a multidimensional Wiener process, while  $K(t) = \{K_k^{(i)}(t)\}_{i \neq k}^{1 \dots Q}$  is a multidimensional bounded variation process (known as a Skorokhod term), increasing only when  $\phi \in \partial \mathcal{T}_Q(\omega_1^{-1})$ . In this section, we report on some experiences of numerical integration of eq. (5.1), performed via the classical Euler integration scheme, first considered in [23]. Technical details follow.

First of all, we obtain the matrix  $C^{(i)}$  numerically by performing a Cholesky factorization of  $B^{(i)}$  at each time integration step. This requires  $B^{(i)}(\bar{\phi})$  to be positive definite for  $\phi \in \mathcal{T}_Q(\omega_1^{-1})$ . Since we lack an analytic proof of this property, we check it numerically. Owing to the inter-clique symmetry given by eq. (4.18), the distribution of the eigenvalue spectrum  $\lambda = \{\lambda_k\}_{k=1}^{Q-1}$  of  $B^{(i)}$  is actually independent of  $i$ . We assume here  $\lambda$  to be increasingly ordered. In Fig. 5, we show the distribution of  $\tau_{\text{FP}} \cdot \lambda$  conditioned to  $\bar{\phi} \sim \mathcal{P}_{\text{FP}}$  at  $(\omega_1, \omega_2) = (2,000.0, 0.3)$  and  $Q = 6$ , as obtained by numerically integrating eq. (5.1) with  $dt = 0.001$  and b.c. type 2 (see below).

Secondly, in sect. 4 we proved that in absence of the Wiener term, the autocorrelation time of eq. (5.1) equals  $\tau_{\text{FP}}$ . We have checked numerically that upon switching the diffusion term on, the autocorrelation time does not change significantly. Therefore, along all numerical integrations we retain only configurations of  $\bar{\phi}$  separated by a number of integration steps

$$\Delta N = k \frac{\tau_{\text{FP}}}{dt}, \quad (5.3)$$

with  $k = 3$  to 4. Some experience shows that integrating the FP equation numerically, with  $\Delta N$  defined as in eq. (5.3), is roughly as much CPU demanding as is simulating the VM.

Finally, we observe that depending on the precise definition of  $K(t)$ , the equilibrium distribution of  $\bar{\phi}(t)$  at finite  $dt$  may be more or less close to  $\mathcal{P}_{\text{FP}}(\bar{\phi})$ . This problem has been investigated in general terms in [24], where a normal reflection scheme at the boundary is adopted and the rate of  $L^p$  convergence of the stochastic process as  $dt \rightarrow 0$  is discussed in full detail. Unfortunately, normal reflections are ill-defined on  $\partial \mathcal{T}_Q(\omega_1^{-1})$  due to the edges of the simplices, thus we cannot follow [24]. Instead, we consider two algorithmic definitions of  $K(t)$ . By letting  $\bar{\phi} \rightarrow \bar{\phi}'$  denote the result of a given Euler integration step with  $\phi \in \mathcal{T}_Q(\omega_1^{-1})$ , we define

- **b.c. type 1** (accept–reject):

- step 1)* if  $(\phi')_{\ell}^{(i)} < 0$  for some  $i, \ell$ , then  $\bar{\phi}'$  is rejected;
- step 2)* if  $\sum_{\ell \neq i}^{1 \dots Q} (\phi')_{\ell}^{(i)} > 1 - \omega_1^{-1}$  for some  $i$ , then  $\bar{\phi}'$  is rejected.

- **b.c. type 2** (boundary projection):

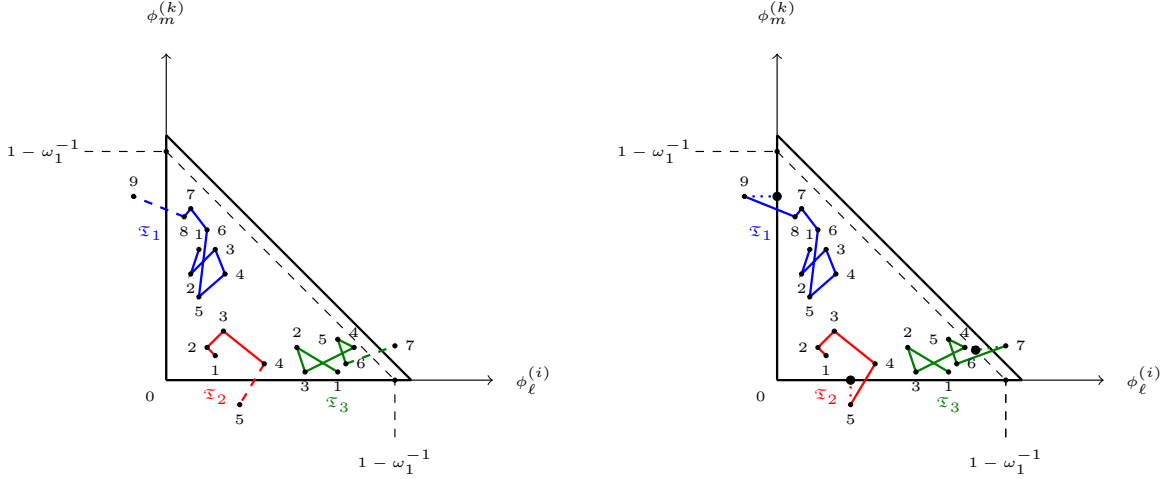


**Figure 6** – *Left*: b.c. type 1. The plot shows schematically three trajectories  $\mathfrak{T}_k$  ( $k = 1, 2, 3$ ) crossing  $\partial\mathcal{T}_Q(\omega_1^{-1})$ . The integration steps  $8 \rightarrow 9$  of  $\mathfrak{T}_1$ ,  $4 \rightarrow 5$  of  $\mathfrak{T}_2$  and  $6 \rightarrow 7$  of  $\mathfrak{T}_3$  are all rejected. *Right*: b.c. type 2. The same trajectories  $\mathfrak{T}_k$  are processed differently. Points 9 of  $\mathfrak{T}_1$ , 5 of  $\mathfrak{T}_2$  and 7 of  $\mathfrak{T}_3$  are projected onto the boundaries. Both plots assume  $m \neq k$  and  $\ell \neq i$ .

- step 1)* if  $(\phi')_\ell^{(i)} < 0$  for some  $i, \ell$ , then we set  $(\phi')_\ell^{(i)} \leftarrow 0$  ;  
*step 2)* if  $\sum_{\ell \neq i}^{1 \dots Q} (\phi')_\ell^{(i)} > 1 - \omega_1^{-1}$  for some  $i$ , then we set  $(\phi')_\ell^{(i)} \leftarrow c \cdot (\phi')_\ell^{(i)}$ , with

$$c = \frac{1 - \omega_1^{-1}}{\sum_{\ell \neq i}^{1 \dots Q} (\phi')_\ell^{(i)}}. \quad (5.4)$$

In Fig. 6 we show schematically some examples of trajectories crossing  $\partial\mathcal{T}_Q(\omega_1^{-1})$  at finite  $dt$ . The plots show how the crossings are handled according to the above recipes. It is easily recognized that b.c. type 1 disfavor updates  $\bar{\phi} \rightarrow \bar{\phi}'$  with  $\bar{\phi}'$  falling closer than  $O(\sqrt{dt})$  to the boundary (recall that  $dt$  is the variance of the increments of a Wiener process). By contrast, b.c. type 2 enhance the rôle of the boundary at finite  $dt$ . We shall see the consequences of this in a moment.

In Fig. 7 (top), we show examples of convergence of the distribution of the excess of votes  $\mathcal{F}_{\text{FP}}(x)$  with b.c. type 1 and type 2 as  $dt \rightarrow 0$  for some values of  $x$ . Data points refer to numerical integrations performed with  $dt = 0.1, 0.01, 0.001$  at  $(\omega_1, \omega_2) = (2,000.0, 0.3)$  and  $Q = 6$ . Statistical uncertainties have been obtained by bootstrapping new distributions from those simulated, with the bin size adopted to measure  $\mathcal{F}_{\text{FP}}(x)$  kept fixed. Lines correspond to combined fits: we model data with b.c. type 1 according to  $y^{(1)} = a + b^{(1)}\sqrt{dt}$  and data with b.c. type 2 according to  $y^{(2)} = a + b^{(2)}\sqrt{dt}$  and then we minimize the overall  $\chi^2$ -function

$$\chi^2 = \sum_{k=1}^3 \left\{ \left[ \frac{y_k^{(\text{b.c. type 1, simulated})} - y_k^{(1)}}{\sigma_k^{(1)}} \right]^2 + \left[ \frac{y_k^{(\text{b.c. type 2, simulated})} - y_k^{(2)}}{\sigma_k^{(2)}} \right]^2 \right\}, \quad (5.5)$$

with respect to  $a$ ,  $b^{(1)}$  and  $b^{(2)}$ . Fits are statistically compatible with a convergence rate of  $\sqrt{dt}$  for both b.c. This result agrees with the findings of [24], despite the different b.c. there considered.

In Fig. 7 (bottom), we compare the distribution of the intra-party excess of votes obtained from the Monte Carlo simulation of the VM at  $(\omega_1, \omega_2) = (2,000.0, 0.3)$  and  $Q = 6$  with the corresponding distributions obtained by numerically integrating eq. (5.1) at the same parameters, with  $dt = 0.1, 0.01, 0.001$  and b.c type 1 and type 2. We see that

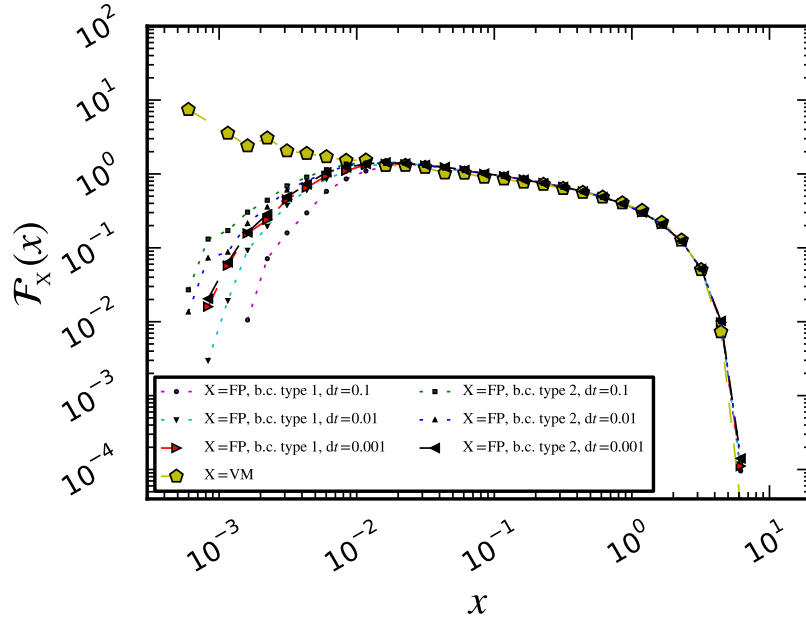
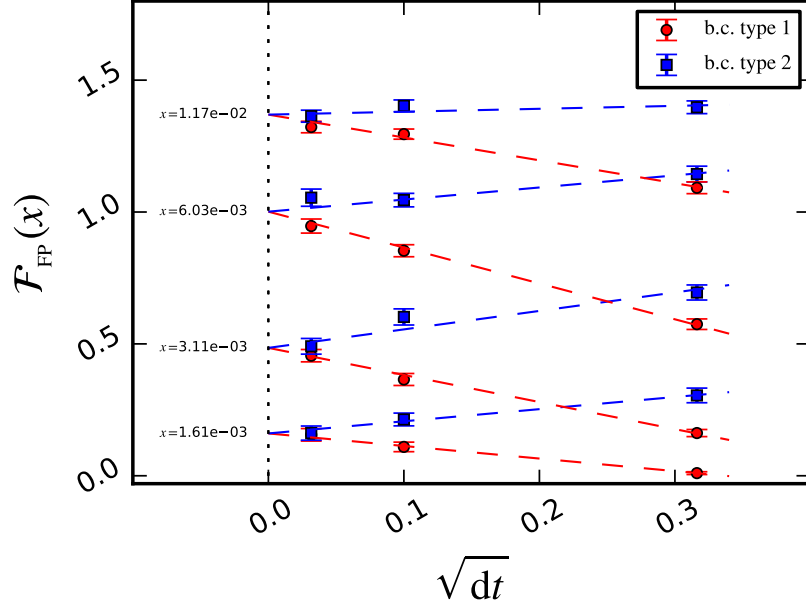


**Figure 7** – *Top*: convergence of  $\mathcal{F}_{\text{FP}}(x)$  with b.c. type 1 and type 2 as  $dt \rightarrow 0$  for some values of  $x$ . Data refer to parameters  $(\omega_1, \omega_2) = (2,000.0, 0.3)$  and  $Q = 6$ . *Bottom*: Comparison between  $\mathcal{F}_{\text{VM}}(x)$  and  $\mathcal{F}_{\text{FP}}(x)$  as obtained by numerical integration of eq. (5.1) for several values of  $dt$ . The plot refers to the same choice of parameters as above.

- all distributions coincide for  $x \gtrsim 0.01$ . Time discretization effects are negligible in this regime, where  $\bar{\phi}(t)$  has larger components on average. Clique MFT matches very well the VM;
- by contrast the distributions obtained from the numerical integration of eq. (5.1) spread out for  $x \lesssim 0.01$ . The lesser  $x$ , the closer  $\bar{\phi}(t)$  lies to  $\partial\mathcal{T}_Q(\omega_1^{-1})$  on average. In practice, the regime of small  $x$  corresponds to probing frequently  $\partial\mathcal{T}_Q(\omega_1^{-1})$ , where boundary reflections become important;
- $\mathcal{F}_{\text{FP}}(x)$  converges from below with b.c. type 1 as  $dt \rightarrow 0$  and from above with b.c. type 2. We have already observed that b.c. type 1 are repulsive, whereas b.c. type 2 are in a sense attractive. Therefore, the former depress  $\mathcal{F}_{\text{FP}}(x)$  at small  $x$  and finite  $dt$ , while the latter enhance it;
- $\mathcal{F}_{\text{FP}}(x)$  has nothing to do with  $\mathcal{F}_{\text{VM}}(x)$  for  $x \lesssim 0.01$ . In sect. 2 we have observed that close to the lower bound  $\omega_1^{-1}$ , the variable  $\phi_k$  is quantized and consequently  $\mathcal{F}_{\text{VM}}(x)$  is a mixture of Dirac delta distributions. Clique MFT assumes  $\phi_k$  to be a continuous variable, thus its probability mass is spread continuously across the whole support  $[\omega_1^{-1}, Q(1 - \omega_1^{-1})]$ . Anyway, at our simulation parameters, the probability content of the region  $[\omega_1^{-1}, 0.01]$  amounts to  $\lesssim 0.01$ , so it does not impact visibly on the shape of the distribution at larger values of  $x$ ;
- an important point which is not discussed in [24] is the dependence of the convergence rate of the stochastic process as  $dt \rightarrow 0$  upon the physical dimension of the convex domain  $\mathcal{D}$ . We observe a strong enhancement of the time discretization effects (the slopes of the curves in Fig. 7 (top)) as  $Q$  increases. This suggests the ansatz

$$\mathbb{E} \|\bar{\phi}(t)|_{dt \neq 0} - \bar{\phi}(t)\| \simeq \gamma(Q)\sqrt{dt}, \quad (5.6)$$

with  $\gamma(Q)$  being a proportionality factor increasing with the number of candidates and depending on the norm considered. Larger values of  $Q$  require smaller values of  $dt$  to keep time discretization effects constant. This makes the numerical integration of eq. (5.1) in the thermodynamic limit highly CPU demanding.

To sum up, clique MFT describes the VM rather well with respect to the autocorrelation times, the average values of the vote variables and the distribution of the excess of votes in the regime where the scaling vote variables can be approximately assumed to be continuous.

## 6 Conclusions

In this paper we explored the stochastic dynamics of the multi-state voter model over a social network, where people belong to cliques dominated by zealot candidates and contacts among different cliques are static and random. In the thermodynamic limit, the model is characterized by two parameters, representing respectively the size of the cliques and the frequency of the random contacts. We studied the equilibrium distribution of the vote variables by means of numerical simulations and analytic arguments based on mean field theory.

In a sense, the model corresponds to a reinterpretation of the *word of mouth* model by Fortunato and Castellano (2007) [1] in a framework where voting is compulsory. The distribution of the intra-party excess of votes observed by us differs significantly from the one characterizing the original word of mouth model, while it resembles roughly that observed in the Brazilian elections: the almost flat shapes pointing towards small values of the scaling vote variable (*cf.* Fig. 4) look phenomenologically encouraging (in a comparison with Fig. 2 of [2]), yet a serious point of weakness is represented by the steepness of the opposite tail. It is difficult to say whether the latter is related to an excessive rigidity of the network considered, an excessive naïvness of the interaction rule or to some other neglected factor. After all,

though inspired by real elections, the model is only a crude approximation of reality (*e.g.* cliques of  $\omega_1 = 1,000$  agents are certainly unrealistic), and its interest lies in its non-trivial dynamics.

It would be interesting to understand how the model depends upon its parameters over a wider spectrum of values than those chosen in this paper and to introduce additional sources of stochasticity (*e.g.* by making the size of the cliques fluctuate). It would be also interesting to simulate the model over different topologies, where the zealot candidates hold positions which are statistically symmetric within the network.

A better understanding of the analytic properties of the distribution of the excess of votes, at least in the context of the Fokker–Planck equation, seems to us unavoidable in order to learn how to improve the model. Some ideas are just sketched in Appendix A, to which the interested reader is referred.

## Acknowledgments

We thank R. Filippini for her participation in the early stage of this work. The computing resources used for our numerical study and the related technical support have been provided by the CRESCO/ENEA-GRID High Performance Computing infrastructure and its staff [25]. CRESCO (C**o**mputational **R**ESearch centre on **C**OMplex systems) is funded by ENEA and by Italian and European research programmes.

## Appendix A On polynomial approximations of $\mathcal{P}_{\text{FP}}(\bar{\phi})$

Eqs. (4.21)–(4.22) show that the coefficient functions  $A_\ell^{(i)}$  and  $B_{\ell m}^{(i)}$  of the FP equation are polynomials of respectively first and second degree in  $\bar{\phi}$ . Since the drift and the diffusion terms involve respectively one and two differentiations, it makes sense to expand  $\mathcal{P}_{\text{FP}}(\bar{\phi})$  in polynomial functions. The polynomial coefficients should be such that the FP equation is fulfilled order by order. Could the maximum degree of the polynomials be finite? To answer this question, it should not be forgotten that the VM collapses to intra-clique consensus as  $\omega_2 \rightarrow 0$ . Although we did not perform numerical integrations of the FP equation in this limit, it is reasonable to expect that

$$\lim_{\omega_2 \rightarrow 0} \mathcal{P}_{\text{FP}}(\bar{\phi}) \simeq \prod_{i=1}^Q \prod_{\ell \neq i}^{1\dots Q} \delta(\phi_\ell^{(i)}). \quad (\text{A.1})$$

If this is correct, the maximum degree of an approximating polynomial should depend on the model parameters and rapidly increase as  $\omega_2 \rightarrow 0$ . Developing polynomial approximations of  $\mathcal{P}_{\text{FP}}(\bar{\phi})$  is a hard task, although polynomials are the most elementary functions one can deal with. Here, we make do with discussing some theoretical aspects of the problem and refer the reader to a future publication for quantitative results [26].

### A.1 Projecting $\mathcal{P}_{\text{FP}}(\bar{\phi})$ onto a basis of Dirichlet distributions

We have seen in sect. 3 that the marginal distributions of  $\phi_\ell^{(i)}$  can be empirically modelled by Beta distributions with very good match. In this respect, eqs. (3.12)–(3.13) are highly suggestive. Recall that a Dirichlet distribution  $\text{Dir}(\alpha)$  of order  $d + 1$  with parameters  $\alpha = \{\alpha_k\}_{k=1}^{d+1}$  has probability density

$$\mathcal{D}_\alpha(x) = \frac{\Gamma(|\alpha|_1)}{\prod_{k=1}^{d+1} \Gamma(\alpha_k)} \left( \prod_{k=1}^d x_k^{\alpha_k - 1} \right) (1 - |x|_1)^{\alpha_{d+1} - 1}, \quad x \in \bar{T}_d, \quad (\text{A.2})$$

$$\bar{T}_d = \{y \in \mathbb{R}_+^d : |y|_1 \leq 1\}. \quad (\text{A.3})$$

It is well known that if  $X \sim \text{Dir}(\alpha)$ , then  $X_i \sim \text{Beta}(\alpha_i, |\alpha|_1 - \alpha_i)$ . Inferring from eqs. (3.12)–(3.13) that the clique vector variable  $\bar{\phi}^{(i)} \equiv \{\phi_k^{(i)}\}_{k \neq i}^{1 \dots Q} \sim \text{Dir}(\alpha, \dots, \alpha, \bar{\alpha}, \alpha, \dots, \alpha)$ , with  $\alpha, \bar{\alpha}$  set according to Table 3 and  $\bar{\alpha}$  being the  $i^{\text{th}}$  component of the parameter vector, could be not far from being correct: at least the argument suggests that Dirichlet distributions might play a relevant rôle in analytic representations of  $\mathcal{P}_{\text{FP}}(\bar{\phi})$ . On a more sound basis, we observe that

$$\text{span} \{ \mathcal{D}_\alpha : \alpha \in \mathbb{N}^{d+1}, |\alpha|_1 = n + d + 1 \} = \text{span} \{ x_1^{\alpha_1} \dots x_d^{\alpha_d} : \alpha \in \mathbb{N}_0^d, |\alpha|_1 \leq n \}, \quad (\text{A.4})$$

*i.e.* Dirichlet distributions with positive integer parameters form a basis of the vector space of multivariate polynomials. Thus, a representation of  $\mathcal{P}_{\text{FP}}(\bar{\phi})$  as a polynomial series can be certainly given in terms of Dirichlet distributions as

$$\mathcal{P}_{\text{FP}}(\bar{\phi}) = \sum_{\underline{\alpha}} c_{\underline{\alpha}} \mathcal{D}_{\underline{\alpha}}(\bar{\phi}), \quad \mathcal{D}_{\underline{\alpha}}(\bar{\phi}) = \mathcal{D}_{\alpha^{(1)}}^{(1)}(\bar{\phi}^{(1)}) \dots \mathcal{D}_{\alpha^{(Q)}}^{(Q)}(\bar{\phi}^{(Q)}), \quad (\text{A.5})$$

$$\mathcal{D}_{\alpha^{(i)}}^{(i)}(\bar{\phi}^{(i)}) \equiv \frac{\Gamma(|\alpha^{(i)}|_1)}{\prod_{k=1}^Q \Gamma(\alpha_k^{(i)})} \left( \prod_{k \neq i}^{1 \dots Q} [\phi_k^{(i)}]^{\alpha_k^{(i)} - 1} \right) \left( 1 - \sum_{k \neq i} \phi_k^{(i)} \right)^{\alpha_i^{(i)} - 1}, \quad (\text{A.6})$$

$$\sum_{\underline{\alpha}} c_{\underline{\alpha}} = 1, \quad (\text{A.7})$$

where the sum in eq. (A.5) extends to all combinations  $\underline{\alpha} = \{\alpha^{(1)}, \dots, \alpha^{(Q)}\} \in \mathbb{N}^{Q \times Q}$  of positive integers. In order to avoid complications, we have deliberately neglected the simplex cut off  $\sum_{k \neq i} \phi_k^{(i)} < 1 - \omega_1^{-1}$  in eq. (A.5): we shall assume for the time being that the support of  $\mathcal{P}_{\text{FP}}(\bar{\phi})$  is  $\mathcal{T}_Q(0)$  instead of  $\mathcal{T}_Q(\omega_1^{-1})$  and come back to this point later on. From eq. (A.5) it follows

$$\mathcal{F}_{\text{FP}}(x) = \int_{\mathcal{T}_Q(0)} \delta(\phi_\ell - x) \mathcal{P}_{\text{FP}}(\bar{\phi}) d\bar{\phi} = \sum_{\underline{\alpha}} c_{\underline{\alpha}} \mathcal{F}_{\underline{\alpha}}(x), \quad (\text{A.8})$$

with

$$\mathcal{F}_{\underline{\alpha}}(x) = \int_{\mathcal{T}_Q(0)} \delta(\phi_\ell - x) \mathcal{D}_{\alpha^{(1)}}^{(1)}(\bar{\phi}^{(1)}) \dots \mathcal{D}_{\alpha^{(Q)}}^{(Q)}(\bar{\phi}^{(Q)}) d\bar{\phi}. \quad (\text{A.9})$$

Before embarking on a determination of the coefficients  $c_{\underline{\alpha}}$  based on the FP equation (which is anyway beyond the scope of this appendix), we should investigate the analytic structure of the integrals  $\mathcal{F}_{\underline{\alpha}}(x)$ . To this aim, we make use of a well known formal trick based on the Fourier representation of the Dirac delta function

$$\delta(x) = \frac{1}{2\pi} \int_{-\infty}^{+\infty} d\lambda e^{i\lambda x}, \quad (\text{A.10})$$

and the formalism of the Laplace transform

$$\mathcal{L}\{f\}(p) = \int_0^\infty e^{-pt} f(t) dt. \quad (\text{A.11})$$

To start with, we observe that by virtue of eq. (2.26) many variables in eq. (A.9) can be integrated out. Accordingly,  $\mathcal{F}_{\underline{\alpha}}(x)$  boils down to

$$\begin{aligned} \mathcal{F}_{\underline{\alpha}}(x) &= \int \delta \left( 1 - x + \sum_{k \neq \ell}^{1 \dots Q} [\phi_\ell^{(k)} - \phi_k^{(\ell)}] \right) \\ &\quad \times \left\{ \prod_{k \neq \ell}^{1 \dots Q} \beta_{\alpha_\ell^{(k)}, |\alpha^{(k)}|_1 - \alpha_\ell^{(k)}}(\phi_\ell^{(k)}) \right\} \mathcal{D}_{\alpha^{(\ell)}}^{(\ell)}(\bar{\phi}^{(\ell)}) \prod_{k \neq \ell}^{1 \dots Q} d\phi_k^{(\ell)} d\phi_\ell^{(k)}. \end{aligned} \quad (\text{A.12})$$

We process separately the three terms under the integral sign. First, we have

$$\delta \left( 1 - x + \sum_{k \neq \ell}^{1 \dots Q} [\phi_\ell^{(k)} - \phi_k^{(\ell)}] \right) = \frac{1}{2\pi} \int_{-\infty}^{\infty} dq e^{iq \{ 1 - x + \sum_{k \neq \ell} [\phi_\ell^{(k)} - \phi_k^{(\ell)}] \}}, \quad (\text{A.13})$$

We then represent  $\mathcal{D}_{\alpha^{(\ell)}}^{(\ell)}(\bar{\phi}^{(\ell)})$  in the equivalent form

$$\begin{aligned} \mathcal{D}_{\alpha^{(\ell)}}^{(\ell)}(\bar{\phi}^{(\ell)}) &= \frac{\Gamma(|\alpha^{(\ell)}|_1)}{\prod_{k=1}^Q \Gamma(\alpha_k^{(\ell)})} \left( \prod_{k \neq \ell}^{1 \dots Q} [\phi_k^{(\ell)}]^{\alpha_k^{(\ell)} - 1} \right) \int_0^\infty [\phi_i^{(\ell)}]^{\alpha_\ell^{(\ell)} - 1} \delta \left( 1 - \sum_{k=1}^Q \phi_k^{(\ell)} \right) d\phi_\ell^{(\ell)} \\ &= \frac{\Gamma(|\alpha^{(\ell)}|_1)}{\prod_{k \neq \ell}^{1 \dots Q} \Gamma(\alpha_k^{(\ell)})} \left( \prod_{k \neq \ell}^{1 \dots Q} [\phi_k^{(\ell)}]^{\alpha_k^{(\ell)} - 1} \right) \frac{1}{2\pi i} \int_{-i\infty}^{+i\infty} \frac{e^{p_0(1 - \sum_{k \neq \ell}^{1 \dots Q} \phi_k^{(\ell)})}}{p_0^{\alpha_\ell^{(\ell)}}} dp_0. \end{aligned} \quad (\text{A.14})$$

In particular, the second line of eq. (A.14) follows from *i*) a rotation of the Fourier integral representing the Dirac delta to the imaginary axis, *ii*) a subsequent exchange of integrals and *iii*) the Laplace transform of monomials. Similarly, we represent the marginal distribution  $\beta_{\alpha_\ell^{(k)}, |\alpha^{(k)}|_1 - \alpha_\ell^{(k)}}(\phi_\ell^{(k)})$  as

$$\beta_{\alpha_\ell^{(k)}, |\alpha^{(k)}|_1 - \alpha_\ell^{(k)}}(\phi_\ell^{(k)}) = \frac{\Gamma(|\alpha^{(k)}|_1)}{\Gamma(\alpha_\ell^{(k)})} \left( \phi_\ell^{(k)} \right)^{\alpha_\ell^{(k)} - 1} \frac{1}{2\pi i} \int_{-i\infty}^{+i\infty} dp \frac{e^{p(1 - \phi_\ell^{(k)})}}{p^{|\alpha^{(k)}|_1 - \alpha_\ell^{(k)}}}. \quad (\text{A.15})$$

In particular, from eq. (A.15) it follows

$$\begin{aligned} \prod_{k \neq \ell}^{1 \dots Q} \beta_{\alpha_\ell^{(k)}, |\alpha^{(k)}|_1 - \alpha_\ell^{(k)}}(\phi_\ell^{(k)}) &= \prod_{k \neq \ell}^{1 \dots Q} \left[ \frac{\Gamma(|\alpha^{(k)}|_1)}{\Gamma(\alpha_\ell^{(k)})} \left( \phi_\ell^{(k)} \right)^{\alpha_\ell^{(k)} - 1} \right] \\ &\cdot \frac{1}{(2\pi i)^{Q-1}} \int_{-i\infty}^{+i\infty} \prod_{k \neq \ell}^{1 \dots Q} \left[ \frac{dp_k}{p_k^{|\alpha^{(k)}|_1 - \alpha_\ell^{(k)}}} \right] e^{\sum_{k \neq \ell} p_k [1 - \phi_\ell^{(k)}]}. \end{aligned} \quad (\text{A.16})$$

The next step is to insert eqs. (A.13), (A.14) and (A.16) into eq. (A.12). Internal integrals over the  $\phi$ 's read

$$\begin{aligned} &\left\{ \prod_{k \neq \ell}^{1 \dots Q} \int_0^\infty d\phi_k^{(\ell)} [\phi_k^{(\ell)}]^{\alpha_k^{(\ell)} - 1} e^{-(iq + p_0)\phi_k^{(\ell)}} \right\} \left\{ \prod_{k \neq \ell}^{1 \dots Q} \int_0^\infty d\phi_\ell^{(k)} [\phi_\ell^{(k)}]^{\alpha_\ell^{(k)} - 1} e^{-(p_k - iq)\phi_\ell^{(k)}} \right\} \\ &= \prod_{k \neq \ell}^{1 \dots Q} \left[ \frac{\Gamma(\alpha_k^{(\ell)})}{(p_0 + iq)^{\alpha_k^{(\ell)}}} \right] \prod_{k \neq \ell}^{1 \dots Q} \left[ \frac{\Gamma(\alpha_\ell^{(k)})}{(p_k - iq)^{\alpha_\ell^{(k)}}} \right]. \end{aligned} \quad (\text{A.17})$$

Thus, we have

$$\begin{aligned} \mathcal{F}_{\underline{\alpha}}(x) &= \frac{\prod_{k=1}^Q \Gamma(|\alpha^{(k)}|_1)}{2\pi} \int_{-\infty}^{+\infty} dq e^{iq(1-x)} \\ &\cdot \frac{1}{2\pi i} \int_{-i\infty}^{+i\infty} dp_0 \frac{1}{p_0^{\alpha_\ell^{(\ell)}}} \prod_{k \neq \ell}^{1 \dots Q} \left[ \frac{1}{(p_0 + iq)^{\alpha_k^{(\ell)}}} \right] e^{p_0 s} \Big|_{s=1} \\ &\cdot \frac{1}{(2\pi i)^{Q-1}} \prod_{k \neq \ell}^{1 \dots Q} \int_{-i\infty}^{+i\infty} dp_k \frac{e^{p_k s}}{p_k^{|\alpha^{(k)}|_1 - \alpha_\ell^{(k)}} (p_k - iq)^{\alpha_\ell^{(k)}}} \Big|_{s=1}. \end{aligned} \quad (\text{A.18})$$

The second and third line of eq. (A.18) are inverse Laplace transforms of products of functions. In order to solve the integrals, one could work out the products in partial fractions or make use of the Laplace

convolution theorem, while recalling that

$$\frac{1}{p_0^{\alpha_\ell^{(\ell)}}} = \mathcal{L} \left\{ f(s) = \frac{s^{\alpha_\ell^{(\ell)}-1}}{\Gamma(\alpha_\ell^{(\ell)})} \right\} (p_0), \quad (\text{A.19})$$

$$\frac{1}{(p_0 + iq)^{\sum_{k \neq \ell} \alpha_k^{(\ell)}}} = \mathcal{L} \left\{ f(s) = \frac{s^{\sum_{k \neq \ell} \alpha_k^{(\ell)}-1} e^{-iqs}}{\Gamma\left(\sum_{k \neq \ell} \alpha_k^{(\ell)}\right)} \right\} (p_0), \quad (\text{A.20})$$

$$(\text{A.21})$$

$$\frac{1}{p_k^{|\alpha^{(k)}|_1 - \alpha_\ell^{(k)}}} = \mathcal{L} \left\{ f(s) = \frac{s^{|\alpha^{(k)}|_1 - \alpha_\ell^{(k)} - 1}}{\Gamma(|\alpha^{(k)}|_1 - \alpha_\ell^{(k)})} \right\} (p_k), \quad (\text{A.22})$$

$$\frac{1}{(p_k - iq)^{\alpha_\ell^{(k)}}} = \mathcal{L} \left\{ f(s) = \frac{s^{\alpha_\ell^{(k)}-1} e^{iqs}}{\Gamma(\alpha_\ell^{(k)})} \right\} (p_k). \quad (\text{A.23})$$

From the Laplace convolution theorem, it follows

$$\begin{aligned} & \frac{1}{2\pi i} \int_{-i\infty}^{+i\infty} dp_0 \frac{e^{p_0 s}}{p_0^{\alpha_\ell^{(\ell)}} (p_0 + iq)^{\sum_{k \neq \ell} \alpha_k^{(\ell)}}} \Big|_{s=1} \\ &= \frac{1}{\Gamma(\alpha_\ell^{(\ell)}) \Gamma(\sum_{k \neq \ell} \alpha_k^{(\ell)})} \int_0^1 d\sigma \sigma^{\sum_{k \neq \ell} \alpha_k^{(\ell)} - 1} (1 - \sigma)^{\alpha_\ell^{(\ell)} - 1} e^{-iq\sigma} \\ &= \frac{1}{\Gamma(|\alpha^{(\ell)}|_1)} M \left( \sum_{k \neq \ell} \alpha_k^{(\ell)}, |\alpha^{(\ell)}|_1, -iq \right), \end{aligned} \quad (\text{A.24})$$

with  $M(a, b, z) = {}_1F_1(a; b; z)$  being the Kummer function. Analogously, we have

$$\begin{aligned} & \frac{1}{(2\pi i)^{Q-1}} \prod_{k \neq \ell}^{1 \dots Q} \int_{-i\infty}^{+i\infty} dp_k \frac{e^{p_k s}}{p_k^{|\alpha^{(k)}|_1 - \alpha_\ell^{(k)}} (p_k - iq)^{\alpha_\ell^{(k)}}} \Big|_{s=1} \\ &= \prod_{k \neq \ell}^{1 \dots Q} \left\{ \frac{1}{\Gamma(\alpha_\ell^{(k)}) \Gamma(|\alpha^{(k)}|_1 - \alpha_\ell^{(k)})} \int_0^1 d\sigma \sigma^{\alpha_\ell^{(k)} - 1} (1 - \sigma)^{|\alpha^{(k)}|_1 - \alpha_\ell^{(k)} - 1} e^{iq\sigma} \right\} \\ &= \prod_{k \neq \ell}^{1 \dots Q} \left\{ \frac{1}{\Gamma(|\alpha^{(k)}|_1)} M \left( \alpha_\ell^{(k)}, |\alpha^{(k)}|_1, iq \right) \right\}. \end{aligned} \quad (\text{A.25})$$

Inserting the right-hand side of eqs. (A.24)–(A.25) back into eq. (A.18) and using the Kummer identity (cf. eq. (13.1.27) of [27])

$$M \left( \sum_{k \neq \ell} \alpha_k^{(\ell)}, |\alpha^{(\ell)}|_1, -iq \right) = e^{-iq} M \left( \alpha_\ell^{(\ell)}, |\alpha^{(\ell)}|_1, iq \right), \quad (\text{A.26})$$

yields

$$\mathcal{F}_{\underline{\alpha}}(x) = \frac{1}{2\pi} \int_{-\infty}^{+\infty} dq e^{-iqx} \prod_{k=1}^Q M \left( \alpha_\ell^{(k)}, |\alpha^{(k)}|_1, iq \right), \quad (\text{A.27})$$

or equivalently (by setting  $p = -iq$ ),

$$\mathcal{F}_{\underline{\alpha}}(x) = \frac{1}{2\pi i} \int_{-i\infty}^{+i\infty} dp e^{px} \prod_{k=1}^Q M \left( \alpha_\ell^{(k)}, |\alpha^{(k)}|_1, -p \right). \quad (\text{A.28})$$

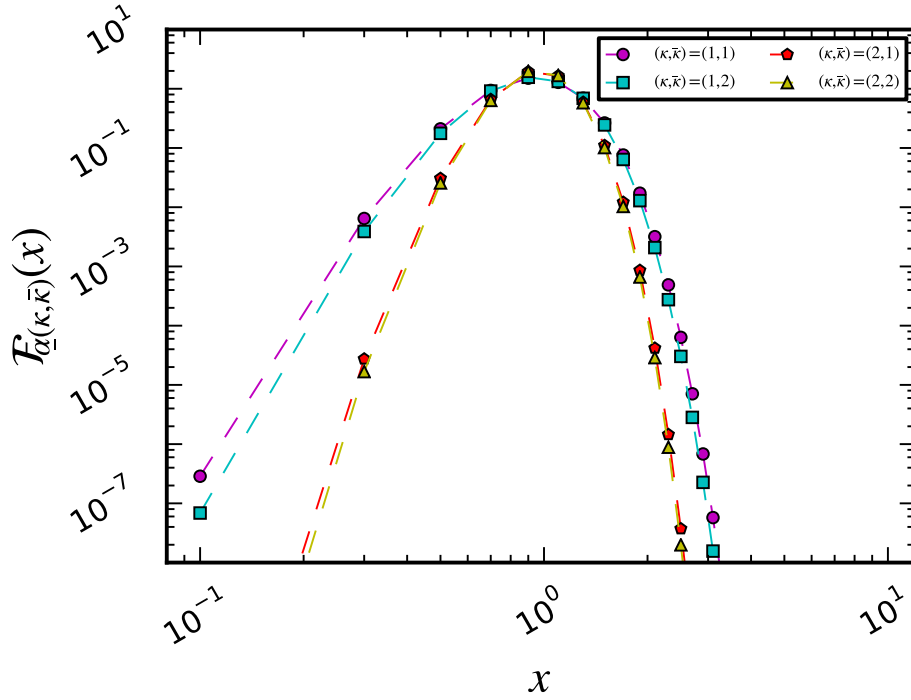


**Figure 8** – Some contributions to  $\mathcal{F}_{\text{FP}}(x)$  arising from a polynomial expansion of  $\mathcal{P}_{\text{FP}}(\bar{\phi})$  based on Dirichlet distributions.

Thus, we see that the contributions to  $\mathcal{F}_{\text{FP}}(x)$  arising from a polynomial expansion of  $\mathcal{P}_{\text{FP}}(\bar{\phi})$  based on Dirichlet distributions are higher transcendental functions. Alternatively, by using once again the Laplace convolution theorem, we can express  $\mathcal{F}_{\underline{\alpha}}(x)$  as a nested integral

$$\begin{aligned} \mathcal{F}_{\underline{\alpha}}(x) = & \int_0^x d\tau_1 \int_0^{\tau_1} d\tau_2 \dots \int_0^{\tau_{Q-2}} d\tau_{Q-1} W(\alpha_\ell^{(\ell)}, |\alpha^{(\ell)}|_1, x - \tau_1) \\ & \cdot W(\alpha_\ell^{(1)}, |\alpha^{(1)}|_1, \tau_1 - \tau_2) \dots W(\alpha_\ell^{(Q)}, |\alpha^{(Q)}|_1, \tau_{Q-1}), \end{aligned} \quad (\text{A.29})$$

with

$$W(a, b, t) = \frac{\Gamma(b)}{\Gamma(a)\Gamma(b-a)} t^{a-1} (1-t)^{b-a-1} \theta(1-t) = \beta_{a,b-a}(t) \theta(1-t), \quad (\text{A.30})$$

and  $\theta(\cdot)$  being the Heaviside step function. Eq. (A.27) can be computed numerically once  $\underline{\alpha}$  is assigned. As an example, we consider the subset of indices

$$\underline{\alpha} = \underline{\alpha}(\kappa, \bar{\kappa}) \equiv \begin{cases} \alpha_j^{(i)} = \kappa, & i \neq j \text{ and } i, j = 1, \dots, Q, \\ \alpha_i^{(i)} = \bar{\kappa}, & i = 1, \dots, Q, \end{cases} \quad (\text{A.31})$$

corresponding to the contributions

$$\mathcal{F}_{\underline{\alpha}(\kappa, \bar{\kappa})}(x) = \frac{1}{2\pi} \int_{-\infty}^{+\infty} dq e^{-iqx} [M(\kappa, \bar{\kappa} + (Q-1)\kappa, iq)]^{Q-1} M(\bar{\kappa}, \bar{\kappa} + (Q-1)\kappa, iq). \quad (\text{A.32})$$

In Fig. (8) we show  $\mathcal{F}_{\underline{\alpha}(\kappa, \bar{\kappa})}$  for some choices of  $(\kappa, \bar{\kappa})$ . We see that all curves lie below  $\mathcal{F}_{\text{FP}}(x)$  by orders of magnitude along the tails, thus suggesting that contributions  $\mathcal{F}_{\underline{\alpha}}(x)$ , where the indices  $\alpha_j^{(i)}$  are not the same for  $i \neq j$ , cannot be neglected.

## A.2 Cutting off the simplex

We finally explore how the Dirichlet distribution changes upon cutting off its defining domain. Specifically, we consider

$$\mathcal{D}_\alpha(x) = Z_\alpha(\omega_1^{-1}) \left( \prod_{k=1}^d x_k^{\alpha_k-1} \right) (1 - |x|_1)^{\alpha_{d+1}-1}, \quad (\text{A.33})$$

as a distribution with support in

$$\bar{T}_d(\omega_1^{-1}) = \{y \in \mathbb{R}_+^d : |y|_1 \leq 1 - \omega_1^{-1}\}. \quad (\text{A.34})$$

The normalization constant  $Z_\alpha(\omega_1^{-1})$  can be calculated analytically according to the same technique used for  $\mathcal{F}_\alpha(x)$  by imposing that the integral of  $\mathcal{D}_\alpha(x)$  over  $\bar{T}_d(\omega_1^{-1})$  equals one. A little algebra yields

$$[Z_\alpha(\omega_1^{-1})]^{-1} = \frac{1}{2\pi i} \int_{-i\infty}^{+i\infty} d\lambda e^{\lambda t} \left( \prod_{i=1}^d \int_0^{+\infty} dx_i x_i^{\alpha_i-1} e^{-\lambda x_i} \right) \int_{\omega_1^{-1}}^{+\infty} dx_{d+1} x_{d+1}^{\alpha_{d+1}-1} e^{-\lambda x_{d+1}} \Big|_{t=1}, \quad (\text{A.35})$$

We notice that

$$\int_{\omega_1^{-1}}^{+\infty} dz z^{\alpha_{d+1}-1} e^{-\lambda z} = \frac{\Gamma(\alpha_{d+1}, \omega_1^{-1}\lambda)}{\lambda^{\alpha_{d+1}}}, \quad (\text{A.36})$$

with  $\Gamma(\alpha_{d+1}, \omega_1^{-1}\lambda)$  denoting the lower incomplete Gamma function. Hence, it follows

$$[Z_\alpha(\omega_1^{-1})]^{-1} = \frac{\prod_{i=1}^d \Gamma(\alpha_i)}{2\pi i} \int_{-i\infty}^{+i\infty} d\lambda e^{\lambda t} \frac{1}{\lambda^\psi} \frac{\Gamma(\alpha_{d+1}, \omega_1^{-1}\lambda)}{\lambda^{\alpha_{d+1}}} \Big|_{t=1}, \quad \psi = \sum_{i=1}^d \alpha_i. \quad (\text{A.37})$$

Once more, the latter integral is the Laplace antitransform of a product of functions. According to the rules of the Laplace transform, it amounts to the convolution of the antitransform of the single functions. Therefore, we have

$$[Z_\alpha(\omega_1^{-1})]^{-1} = \frac{\prod_{i=1}^{d+1} \Gamma(\alpha_i)}{\Gamma(|\alpha|_1)} I_{\psi, \alpha_{d+1}}(1 - \omega_1^{-1}) = [Z_\alpha(0)]^{-1} I_{\psi, \alpha_{d+1}}(1 - \omega_1^{-1}), \quad (\text{A.38})$$

where

$$I_{a,b}(z) = \int_0^z d\tau \beta_{a,b}(\tau), \quad (\text{A.39})$$

denotes the regularized incomplete beta function. Since this has an asymptotic expansion at  $z = 1$

$$I_{a,b}(z) = 1 - \frac{(1-z)^b z^a}{b B_{a,b}} \sum_{k=0}^{\infty} \frac{(-1)^k (a+b)_k (z-1)^k}{(b+1)_k}, \quad b \neq -1, \quad (\text{A.40})$$

with  $B_{a,b} = \Gamma(a)\Gamma(b)/\Gamma(a+b)$ , we conclude that

$$[Z_\alpha(\omega_1^{-1})]^{-1} = [Z_\alpha(0)]^{-1} + \mathcal{O}[(\omega_1^{-1})^{\alpha_{d+1}}]. \quad (\text{A.41})$$

Thus, we see that depending on  $\alpha_{d+1}$ , the impact of cutting off the integration domain (the Cartesian product of simplices), at the boundary on the Dirichlet integrals could be very small.

## References

- [1] S. Fortunato and C. Castellano. Scaling and Universality in Proportional Elections. *Physical Review Letters*, 99(13):138701, 2007.
- [2] A. Chatterjee, M. Mitrović, and S. Fortunato. Universality in voting behavior: an empirical analysis. *Scientific Reports*, 3, 2013.
- [3] R. N. Costa Filho, M. P. Almeida, J. S. Andrade, and J. E. Moreira. Scaling behavior in a proportional voting process. *Physical Review E*, 60(1):1067–1068, 1999.
- [4] P. Clifford and A. Sudbury. A model for spatial conflict. *Biometrika*, 60(3):581–588, 1973.
- [5] R. Holley and T. M. Liggett. Ergodic theorems for weakly interacting infinite systems and the voter model. *The Annals of Probability*, 3(4):643–663, 1975.
- [6] G. A. Böhme and T. Gross. Fragmentation transitions in multistate voter models. *Physical Review E*, 85:066117, 2012.
- [7] S. P. Hubbell. *The Unified Neutral Theory of Biodiversity and Biogeography (MPB-32) (Monographs in Population Biology)*. Princeton University Press, 2001.
- [8] A. J. McKane, D. Alonso, and R. V. Solé. Analytic solution of hubbell’s model of local community dynamics. *Theoretical Population Biology*, 65(1):67 – 73, 2004.
- [9] S. Pigolotti, A. Flammini, M. Marsili, and A. Maritan. Species lifetime distribution for simple models of ecologies. *Proceedings of the National Academy of Sciences USA*, 102(44):15747–51+, 2005.
- [10] M. Starnini, A. Baronchelli, and R. Pastor-Satorras. Ordering dynamics of the multi-state voter model. *Journal of Statistical Mechanics*, P10027, 2012.
- [11] M. Mobilia. Does a single zealot affect an infinite group of voters? *Physical Review Letters*, 91:028701, 2003.
- [12] D. Acemoglu, G. Como, F. Fagnani, and A. E. Ozdaglar. Opinion fluctuations and disagreement in social networks. Levine’s working paper archive, D. K. Levine, 2010.
- [13] E. Yildiz, D. Acemoglu, A. E. Ozdaglar, A. Saberi, and A. Scaglione. Discrete opinion dynamics with stubborn agents. *LIDS report 2858, to appear in ACM Transactions on Economics and Computation*, 2012.
- [14] Y. Wu and J. Shen. Opinion dynamics with stubborn vertices. *Electronic Journal of Linear Algebra*, 23:790–800, 2012.
- [15] J. Xie, S. Sreenivasan, G. Korniss, W. Zhang, C. Lim, and B. K. Szymanski. Social consensus through the influence of committed minorities. *Physical Review E*, 84(1):011130, 2011.
- [16] J. Xie, J. Emenheiser, M. Kirby, S. Sreenivasan, B. K. Szymanski, and G. Korniss. Evolution of opinions on social networks in the presence of competing committed groups. *PLoS ONE*, 7(3):e33215, 2012.
- [17] P. Singh, S. Sreenivasan, B. K. Szymanski, and G. Korniss. Accelerating consensus on coevolving networks: The effect of committed individuals. *Physical Review E*, 85:046104, 2012.
- [18] M. Mobilia. Commitment Versus Persuasion in the Three-Party Constrained Voter Model. *Journal of Statistical Physics*, 151:69–91, 2013.

- [19] D. J. Watts and S. H. Strogatz. Collective dynamics of “small–world” networks. *Nature*, 393(6684):409–10, 1998.
- [20] C. W. Gardiner. *Handbook of Stochastic Methods*. Springer Series in Synergetics. Springer, 1994.
- [21] M. Bastian, S. Heymann, and M. Jacomy. Gephi: An open source software for exploring and manipulating networks, 2009.
- [22] M. Mobilia, A. Petersen, and S. Redner. On the role of zealotry in the voter model. *Journal of Statistical Mechanics: Theory and Experiment*, 2007(08):P08029+, 2007.
- [23] G. Maruyama. Continuous Markov processes and stochastic equations. *Rendiconti del Circolo Matematico di Palermo*, 4(1):48–90, 1955.
- [24] L. Słomiński. On approximation of solutions of multidimensional sde’s with reflecting boundary conditions. *Stochastic Processes and their Applications*, 50(2):197–219, 1994.
- [25] see <http://www.cresco.enea.it/english> for information.
- [26] F. Palombi and S. Toti. Work in progress.
- [27] M. Abramowitz and I. A. Stegun. *Handbook of Mathematical Functions with Formulas, Graphs, and Mathematical Tables*. Dover Publications, New York, 1964.